FIESTA Lecture Notes by *Jørgen Randrup* (LBNL)
September 17, 2014

Fission Dynamics within the Macroscopic-Microscopic Approach

Shortly after the discovery of nuclear fission [1], it was recognized that the phenomenon can be viewed as an *evolution of the nuclear shape* from that of a single compound nucleus to that of two receding fragments [2, 3]. This conceptual framework, when combined with the macroscopic-microscopic approach to the calculation of nuclear energetics, provides a powerful and quantitatively useful theoretical tool for studies of low-energy fission dynamics. These lectures give an introduction to the treatment of nuclear fission dynamics within the macroscopic-microscopic approach.

The first lecture discusses the general features of the problem, including the concept of shape degrees of freedom and the formal framework for treating their dynamical evolution. It will also describe the most common approach to calculating of the nuclear macroscopic-microscopic potential energy of deformation.

The second lecture focuses on the dynamical evolution of the fissioning nucleus. The inertial mass associated with the shape motion as well as the dissipative coupling between the shape and the residual system will be discussed and recent advances in the treatment of the nuclear dynamics will be highlighted, with particular emphasis on the simplifications that arise when the dissipation is strong.

Contents

1 Introduction **2**

2 Formal framework for nuclear shape dynamics **3**
2.1 Temperature 5
2.2 Equilibration 6

3 Shape families **7**
3.1 Expansion in Legendre polynomials 7
3.2 Three quadratic surfaces of revolution 7

4 Potential energy **8**
4.1 Macroscopic energy 10
4.2 Shell-plus-pairing energy 12
4.3 Calculated results 16

5 Inertial mass **19**

6 Dissipation **20**
6.1 One-body dissipation in a mononucleus 21
6.2 One-body dissipation in a dinucleus 21
6.3 Average macroscopic fission dynamics 22

7 Fission dynamics **23**
7.1 Smoluchowski limit 24
7.2 Metropolis lattice walk 26
7.3 Langevin simulations 27

1 Introduction

Various basic properties of nuclei of particular relevance to fission dynamics:

Nuclear saturation: The nucleon-nucleon interaction has a finite range with an attractive component (mediated by the pion) and a short-range repulsion (mediated by heavier mesons). Consequently nuclear matter saturates and nuclei are approximately *incompressible* as well as *leptodermous* (have a thin skin): As a result, the nucleus can be regarded as having a *shape*.

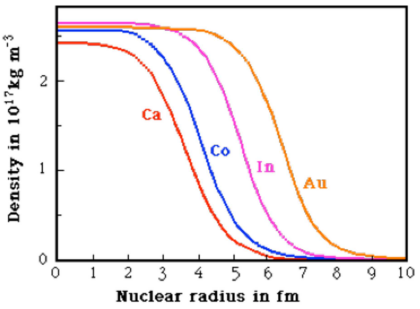

Figure 1-1: The nuclear density profile for nuclei of various mass number: The bulk region has a density close to that of nuclear matter, and the nuclear surface has a constant width that is substantially smaller than the nuclear radius, $w \ll R \sim A^{1/3}$.

Compound nucleus: The internal relaxation is much faster than the time scales characteristic of the nuclear disintegration processes, so the microscopic degrees of freedom can be regarded as being in approximate equilibrium [4].

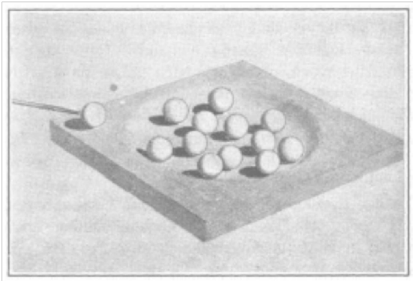

Figure 1-2: Illustration of absorption of a neutron by a nucleus: The impinging neutron (left) induces a cascade of collisions that leads to a quick sharing its energy among all the nucleons (from Ref. [5]). Part of the excitation energy may later become concentrated on a single nucleon, causing it to be emitted [4], or it may be converted to deformation energy, allowing the nuclear shape to develop beyond the fission barrier [3].

Shape dynamics: Nuclear fission can be understood as a dynamical evolution of the nuclear shape [3], subject to both conservative and dissipative forces.

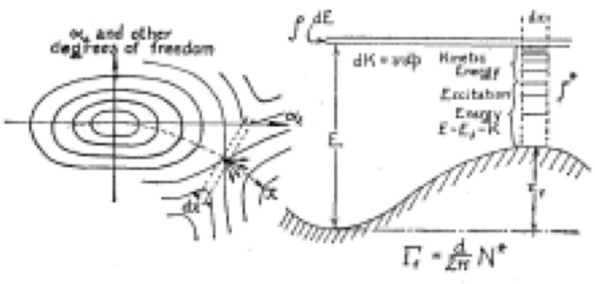

Figure 1-3: Schematic contour diagram of the potential energy of deformation. Agitations of the nucleus results in shape excursions away from the ground-state minimum. If the excitaiton is sufficient, the shape motion will eventually traverse the fission barrier and nuclear fission will result; its rate can be estimated by statistical means (known as the transition-state method). (From Ref. [3].)

2 Formal framework for nuclear shape dynamics

The nuclear system is defined in terms of its *shape*. This is possible because the nuclear interaction has a finite range and leads to saturation. As a consequence, the density of nucleons, $\rho(\boldsymbol{r})$, is rather constant in the interior of a large nucleus and falls off over a relatively short distance at the surface. The task of theory is to describe the temporal evolution of the nuclear shape.

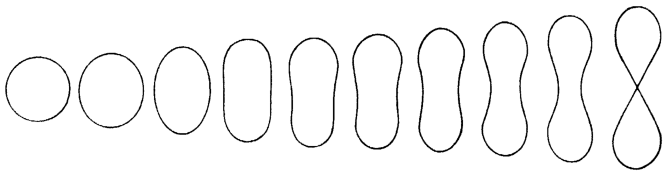

Figure 2-4: Reflection-symmetric nuclear shapes relevant for fission, starting from a single sphere and ending with a scission shape.

The nuclear shape [Sect. 3] is specified by a set of *shape parameters* $\boldsymbol{q} \equiv (q_1, \ldots, q_N)$, often referred to as the collective degrees of freedom. Generally, for any given total energy E, the specification of $\boldsymbol{q}$ characterizes an entire ensemble of nuclear many-body states that all have the energy E and whose spatial density distributions all correspond to the specified shape. Assuming that all such states are equally likely, the system may be considered as being in statistical equilibrium.

The calculation of the time evolution of the nuclear shape parameters, $\boldsymbol{q}(t)$, requires knowledge of three distinct physical quantities:

1. **Potential energy:** [Sect. 4] The most basic quantity is the potential energy of a given shape, $U(\boldsymbol{q})$, *i.e.* the energy of the nuclear system when its shape is as specified by $\boldsymbol{q}$. The local gradient of the potential energy provides a driving force, $\boldsymbol{F}(\boldsymbol{q}) = -\partial U(\boldsymbol{q})/\partial \boldsymbol{q}$, that will seek to change the shape so that the potential energy is lowered. The minima in the potential-energy surface of a given nucleus correspond to stable equilibrium shapes; the lowest compact minimum represents the ground state and its energy is the nuclear mass. Two-dimensional contour plots have intuitive appeal, displaying minima, ridges, saddle points, and so on) but cannot bring out all important features of the N-dimensional space.

2. **Inertial mass:** [Sect. 5] A shape change is associated with a rearrangement of the internal nucleonic configurations. The associated kinetic energy is assumed to be of normal form, $K = \frac{1}{2}\sum_{i,j}^{N} M_{ij}\dot{q}_i\dot{q}_j$, where $\boldsymbol{M}(\boldsymbol{q})$ is the $N \times N$ inertial-mass tensor which is symmetric, $M_{ij}(\boldsymbol{q}) = M_{ji}(\boldsymbol{q})$. Thus $\boldsymbol{M}(\boldsymbol{q})$ consists of $N \times (N+1)/2$ independent functions of $\boldsymbol{q}$.

3. **Dissipation:** [Sect. 6] The interaction between the collective degrees of freedom and the remainder of the nuclear many-body system causes the shape variables to experience a dissipative force characterized by the $N \times N$ *dissipation tensor* $\boldsymbol{\gamma}(\boldsymbol{q})$, which is symmetric, $\gamma_{ij}(\boldsymbol{q}) = \gamma_{ji}(\boldsymbol{q})$. Thus $\boldsymbol{\gamma}(\boldsymbol{q})$ consists of $N \times (N+1)/2$ independent functions of $\boldsymbol{q}$.

If the shape evolution took place in isolation, *i.e.* if there were no coupling between the shape variables $\boldsymbol{q}$ and the internal degrees of freedom, then the shape dynamics would be conservative. The time evolution of the shape would then follow exclusively from the Lagrangian function,

$$\mathcal{L}(\boldsymbol{q},\dot{\boldsymbol{q}}) \;=\; \tfrac{1}{2}\dot{\boldsymbol{q}}\cdot\boldsymbol{M}\cdot\dot{\boldsymbol{q}} - U(\boldsymbol{q}) \;=\; \tfrac{1}{2}\sum_{i,j}^{N}\dot{q}_i\,M_{ij}(\boldsymbol{q})\,\dot{q}_j - U(\boldsymbol{q})\;. \tag{2-1}$$

The conjugate shape momentum $\boldsymbol{p} = (p_1, \ldots, p_N)$ is given in terms of $\boldsymbol{q}$ and $\dot{\boldsymbol{q}}$ as

$$p_i(\boldsymbol{q}, \dot{\boldsymbol{q}}) \;=\; \frac{\partial}{\partial \dot{q}_i} \mathcal{L}(\boldsymbol{q}, \dot{\boldsymbol{q}}) \;=\; \sum_j M_{ij}(\boldsymbol{q})\, \dot{q}_j : \;\; \boldsymbol{p}(\boldsymbol{q}, \dot{\boldsymbol{q}}) \;=\; \boldsymbol{M}(\boldsymbol{q}) \cdot \dot{\boldsymbol{q}} \;. \tag{2-2}$$

This relation can be inverted to yield the velocity $\dot{\boldsymbol{q}}$ in terms of $\boldsymbol{q}$ and $\boldsymbol{p}$,

$$\dot{q}_i(\boldsymbol{p}, \boldsymbol{q}) = \sum_j B_{ij}(\boldsymbol{q})\, p_j : \;\; \dot{\boldsymbol{q}}(\boldsymbol{p}, \boldsymbol{q}) \;=\; \boldsymbol{B}(\boldsymbol{q}) \cdot \boldsymbol{q} \;, \tag{2-3}$$

where the $N \times N$ matrix $\boldsymbol{B}(\boldsymbol{q})$ denotes the inverse of $\boldsymbol{M}(\boldsymbol{q})$, *i.e.* $\sum_j B_{ij}(\boldsymbol{q}) M_{jk}(\boldsymbol{q}) = \delta_{ik}$. The Lagrange equation of motion for the evolution of the shape momentum is

$$\frac{\partial}{\partial t} p_i \;\doteq\; \frac{\partial}{\partial q_i} \mathcal{L}(\boldsymbol{q}, \dot{\boldsymbol{q}}) \;=\; \tfrac{1}{2} \sum_{jk} \dot{q}_j \dot{q}_k \frac{\partial}{\partial q_i} M_{jk}(\boldsymbol{q}) - \frac{\partial}{\partial q_i} U(\boldsymbol{q}) \;. \tag{2-4}$$

The conservative shape dynamics can equally well be described within the Hamiltonian formalism. The Hamiltonian function for the shape motion is given by

$$\mathcal{H}(\boldsymbol{p}, \boldsymbol{q}) \;=\; \tfrac{1}{2} \boldsymbol{p} \cdot \boldsymbol{B} \cdot \boldsymbol{p} + U(\boldsymbol{q}) \;=\; \tfrac{1}{2} \sum_{i,j}^{N} p_i B_{ij}(\boldsymbol{q})\, p_j + U(\boldsymbol{q}) \tag{2-5}$$

and the Hamiltonian equations of motion are

$$\begin{aligned} \dot{q}_i \;&=\; \frac{\partial}{\partial p_i} \mathcal{H}(\boldsymbol{p}, \boldsymbol{q}) = \sum_j B_{ij}(\boldsymbol{q})\, p_j \;, \\ \dot{p}_i \;&=\; -\frac{\partial}{\partial q_i} \mathcal{H}(\boldsymbol{p}, \boldsymbol{q}) = -\tfrac{1}{2} \sum_{j,k}^{N} p_j p_k \frac{\partial}{\partial q_i} B_{jk}(\boldsymbol{q}) - \frac{\partial}{\partial q_i} U(\boldsymbol{q}) = F_i^{\rm cons} = F_i^{\rm mass}(\boldsymbol{p}, \boldsymbol{q}) + F_i^{\rm pot}(\boldsymbol{q}) \;. \end{aligned}$$

It is easy to verify that the Hamiltonian and Lagrangian equations of motion are equivalent (it follows from the fact that $\sum_{jk} p_j p_k \partial B_{jk}/\partial q_i = -\sum_{jk} \dot{q}_j \dot{q}_k \partial M_{jk}/\partial q_i$). In either formulation, the conservative force consists not only of the *driving force* provided by the potential, $\boldsymbol{F}^{\rm pot}(\boldsymbol{q}) \equiv -\partial U(\boldsymbol{q})/\partial \boldsymbol{q}$, but has also contributions arising from the shape dependence of the inertial mass, $\boldsymbol{F}^{\rm mass}(\boldsymbol{q})$. If the shape motion were conservative, then the associated energy, $E_{\rm coll} = \mathcal{H}(\boldsymbol{p}, \boldsymbol{q})$ would remain constant in time. 2-a

However, there is a continual exchange of energy between the retained collective degrees of freedom and the remainder of the system and, as a consequence, the shape cannot be considered as an isolated system. Rather, it displays a dissipative evolution. The interaction of the shape degrees of freedom with the remainder of the system is described by means of a residual force which is dissipative, $\boldsymbol{F}^{\rm diss}(\dot{\boldsymbol{q}}, \boldsymbol{q})$. Its average exerts a friction force on the shape parameters $\boldsymbol{q}$,

$$\boldsymbol{F}^{\rm fric}(\boldsymbol{q}, \dot{\boldsymbol{q}}) \equiv \langle \boldsymbol{F}^{\rm diss}(\boldsymbol{q}, \dot{\boldsymbol{q}}) \rangle = -\boldsymbol{\gamma}(\boldsymbol{q}) \cdot \dot{\boldsymbol{q}} : \quad F_i^{\rm fric}(\boldsymbol{q}, \dot{\boldsymbol{q}}) = \langle F_i^{\rm diss}(\boldsymbol{q}, \dot{\boldsymbol{q}}) \rangle = -\sum_j \gamma_{ij}(\boldsymbol{q})\, \dot{q}_j \;. \tag{2-6}$$

It can be obtained from the Rayleigh function $\mathcal{F}(\boldsymbol{q}, \dot{\boldsymbol{q}})$, equal to half the mean rate of dissipation,

$$F_i^{\rm fric}(\boldsymbol{q}, \dot{\boldsymbol{q}}) \;=\; -\frac{\partial}{\partial \dot{q}_i} \mathcal{F}(\dot{\boldsymbol{q}}, \boldsymbol{q}) \;, \;\; \mathcal{F}(\dot{\boldsymbol{q}}, \boldsymbol{q}) \;=\; \tfrac{1}{2} \dot{\boldsymbol{q}} \cdot \gamma(\boldsymbol{q}) \cdot \dot{\boldsymbol{q}} \;=\; \tfrac{1}{2} \sum_{ij} \dot{q}_i \gamma_{ij}(\boldsymbol{q})\, \dot{q}_j \;. \tag{2-7}$$

The remainder of the dissipative force, $\boldsymbol{F}^{\rm ran}(\boldsymbol{q},t) \equiv \boldsymbol{F}^{\rm diss}(\dot{\boldsymbol{q}},\boldsymbol{q}) - \boldsymbol{F}^{\rm fric}(\dot{\boldsymbol{q}},\boldsymbol{q})$ is stochastic in nature. It is assumed to fluctuate rapidly in time and to be *Markovian* (*i.e.* it has vanishing memory time), so its autocorrelation function is given by

$$\langle \boldsymbol{F}^{\rm ran}(\boldsymbol{q},t)\boldsymbol{F}^{\rm ran}(\boldsymbol{q},t')\rangle = 2\boldsymbol{\gamma}(\boldsymbol{q})\,T\,\delta(t-t') : \quad \langle F_i^{\rm ran}(\boldsymbol{q},t)F_j^{\rm ran}(\boldsymbol{q},t')\rangle = 2\gamma_{ij}(\boldsymbol{q})\,T\,\delta(t-t') \ , \quad \text{(2-8)}$$

where $T(\boldsymbol{q},\dot{\boldsymbol{q}})$ is the temperature of the residual system [Sect. 2.1]. The fact that the mean and the variance of the residual force are both proportional to the dissipation tensor is a manifestation of the *fluctuation-dissipation theorem* (often referred to as the *Einstein relation*) which ensures that the system equilibrates appropriately [Sect. 2.2].

The resulting complete equation of motion for the evolution of the shape parameters is then given by the *Langevin* equation,

$$\dot{\boldsymbol{p}} \ = \ \boldsymbol{F}^{\rm cons} + \boldsymbol{F}^{\rm diss} \ = \ \Big(\boldsymbol{F}^{\rm mass}(\boldsymbol{p},\boldsymbol{q}) + \boldsymbol{F}^{\rm pot}(\boldsymbol{q})\Big) \ + \ \Big(\boldsymbol{F}^{\rm fric}(\boldsymbol{q},\dot{\boldsymbol{q}}) + \boldsymbol{F}^{\rm ran}(\boldsymbol{q},t)\Big) \ . \quad \text{(2-9)}$$

In this description, the conservative motion on the potential-energy landscape is subjected to a steady damping caused by the friction force (which is the average effect of the residual coupling) and, importantly, the shape trajectory $\boldsymbol{q}(t)$ exhibits continual random changes due to the fluctuating part of the residual coupling. Because of this diffusive character of the evolution, a specified initial shape automatically develops into an entire ensemble of (often very) different shapes. Such occurrence of trajectory branching is a general feature of the transport description and it is a key advantage of this type of treatment because fission of a single compound nucleus may have many macroscopically different outcomes (for example: different mass splits and different fragment kinetic energies). In particular, without a diffusive term the equation of motion could never lead to asymmetric fission if the initial nucleus had reflection symmetry.

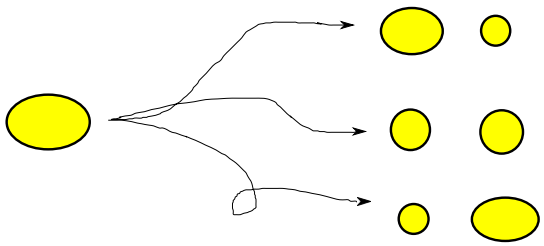

Figure 2-5: Illustration of how a single shape may develop into a multitude of qualitatively different shapes due to the coupling between the shape degrees of freedom treated explicitly and those of the residual system.

2.1 Temperature

The total energy of the evolving nuclear system, E, can be divided into collective and statistical parts. In the absense of overall rotation (which we assume throughout here), the collective energy consists of the potential energy of the given shape, $U(\boldsymbol{q})$, plus the kinetic energy associated with the rate of shape change, $K(\boldsymbol{q},\dot{\boldsymbol{q}})$,

$$E_{\rm coll}(\boldsymbol{q},\dot{\boldsymbol{q}}) \ = \ \tfrac{1}{2}\sum_{ij}\dot{q}_i M_{ij}(\boldsymbol{q})\,\dot{q}_j + U(\boldsymbol{q}) \ . \quad \text{(2-10)}$$

The remainder is the statistical energy,

$$E_{\rm stat}(\boldsymbol{q},\dot{\boldsymbol{q}}) = \ E - E_{\rm coll}(\boldsymbol{q},\dot{\boldsymbol{q}}) \ , \quad \text{(2-11)}$$

from which the *local* temperature, $T(\boldsymbol{q},\dot{\boldsymbol{q}})$, can be obtained. For example, $E_{\rm stat}(\boldsymbol{q}) = a_A T(\boldsymbol{q},\dot{\boldsymbol{q}})^2$ in a simple Fermi-gas model, where $a_A \approx A/(8\,{\rm MeV})$ is the nuclear level-density parameter.

2.2 Equilibration

The presence of the dissipative term in the Langevin equation of motion (2-9) is instrumental in ensuring that a closed system develops towards statistical equilibrium. To illustrate this central feature of the Langevin dynamical framework, let us consider a "particle" having a constant mass m moving in a simple one-dimensional harmonic potential, $U(x) = \frac{1}{2}c_0x^2$, while in contact with a thermal reservoir of temperature T; let γ be the associated dissipation coefficient. The driving force is then $F^{\rm pot} = -\partial U/\partial x = -c_0x$, while the friction force is $F^{\rm fric} = -\gamma\dot{x}$, so the average position $\bar{x} = \langle x\rangle$ evolves as a damped harmonic oscillator, $m\ddot{\bar{x}}+\gamma\dot{\bar{x}}+c_0\bar{x} = 0$, and thus approaches zero in the course of time, $\bar{x}(t) \to 0$. The random force satisfies $\langle F^{\rm ran}(t)F^{\rm ran}(t')\rangle = 2\gamma T\delta(t-t')$ and produces fluctuations around the mean trajectory $\bar{x}(t)$. It is elementary to show that $\langle x^2\rangle \to T/c_0$ and $\langle \dot{x}^2\rangle \to T/m$, consistent with the fact the evolving distribution function $P(x,\dot{x},t)$ approaches that of thermal equilibrium, $P_T(x,\dot{x}) \sim \exp(-(m\dot{x}^2 + c_0x^2)/2T)$.

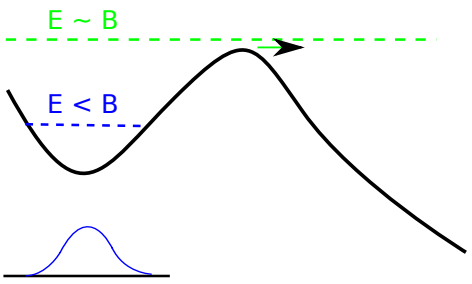

Figure 2-6: Schematic potential energy of deformation $U(Q)$ (the minimum energy at the specified quadrupole moment Q); the ground state is at the minimum and the fission barrier is at the maximum. When the total energy E is below the barrier the shape distribution produced by the Langevin equation approaches statistical equilibrium (sketched below the minimum). When the energy is slightly above the barrier the shape attains quasi-equilibrium inside the barrier, while there is a slow leakage across the barrier towards fission; the fission rate can be calculated statistically leading to the transition-state expression.

In the Smoluchowski limit (Sect. 7.1) the dissipation is so strong that the inertial forces are negligible, equivalent to putting the inertial mass to zero. The instantaneous velocity is then given by $\dot{x}(t) = \mu[F^{\rm pot}(x) + F^{\rm ran}(x,t)]$, where the *mobility coefficient* is $\mu = 1/\gamma$. The distribution, $P(x,t)$, satisfies the *Fokker-Planck equation*,

$$\partial_t P(x,t) \;=\; -\partial_x V(x)P(x,t) + \partial_x^2 D(x)P(x,t)\ , \tag{2-12}$$

where the transport coefficients satisfy the *Einstein relation*, $VT = DF$. In the harmonic case, the *drift coefficient* is linear, $V(x) = -\mu c_0 x = -x/t_0$, with $t_0 = \gamma/c_0$ being the *relaxation time*, while the *diffusion coefficient* is constant, $D = \mu T = T/c_0t_0$. Then

$$\frac{d}{dt}\bar{x} = V(\bar{x}) = -\frac{\bar{x}}{t_0} \;\Rightarrow\; \bar{x}(t) = x(0)\,{\rm e}^{-t/t_0} \to 0\ , \tag{2-13}$$

$$\frac{d}{dt}\sigma^2 = 2D - \frac{2}{t_0}\sigma^2 \;\Rightarrow\; \sigma^2(t) = Dt_0(1-{\rm e}^{-2t/t_0}) + \sigma^2(0)\,{\rm e}^{-2t/t_0} \to Dt_0 = T/c_0\ . \tag{2-14}$$

The mean position $\bar{x} \equiv \langle x\rangle$ relaxes exponentially, while the variance $\sigma^2 \equiv \langle (x-\bar{x})^2\rangle$ grows linearly at early times, $\sigma^2(t \ll t_0) \approx 2Dt$. The distribution approaches equilibrium at late times, $t \gg t_0$, and if it is initially sharp then it remains a Gaussian at all times, 2-b

$$P(x,0) = \delta(x-x_0):\ P(x,t) = \Big[2\pi\sigma^2(t)\Big]^{-\frac{1}{2}}\,{\rm e}^{-[x-\bar{x}(t)]^2/2\sigma^2(t)} \to \left[\frac{c_0}{2\pi T}\right]^{\frac{1}{2}}{\rm e}^{-c_0x^2/2T}\ . \tag{2-15}$$

3 Shape families

Many different shape families have been employed in fission studies. In the present lectures, we restrict the considerations to shapes that have rotational symmetry around the z axis (deviations from such "axial" symmetry are known to play a significant role near the first fission barrier) and we discuss just two of them here.

3.1 Expansion in Legendre polynomials

Axially symmetric shapes in the vicinity of a sphere can be described by $R(\vartheta)$, the distance from the nuclear center to the surface. It is convenient to expand this function in Legendre polynomials,

$$R(\vartheta) \;=\; R_0 \left[1 + \sum_{n\geq 1} \alpha_n P_n(\vartheta) \right] / \lambda(\alpha_1, \alpha_2, \ldots) \;, \tag{3-1}$$

where the normalization constant λ ensures that the enclosed volume remains equal to $\frac{4}{3}\pi R_0^3$. Roughly speaking, α_2 controls the quadrupole moment, α_3 the mass asymmetry, and α_4 the neck thickness. While such parametrizations are very suitable for small distortions away from a sphere, they grow progressively impractical as the fissioning nucleus develops large distortions for which many terms would be required. (Eventually, as scission is approached, the approach may even break down entirely because the function $R(\vartheta)$ may then no longer be single-valued.)

3.2 Three quadratic surfaces of revolution

In general, an axially symmetric shape can be characterized by $\rho(z)$. In the 3QS parametrization, the shape is given by three smoothly joined quadratic surfaces [6], so $\rho^2(z)$ is of the form

$$\rho^2(z) = \begin{cases} L: \; a_1^2 - (a_1^2/c_1^2)(z-\ell_1)^2, & z_0 \leq z \leq z_1 \;\; : \;\; \rho\partial_z\rho = -(a_1^2/c_1^2)(z-\ell_1) \;, \\ M: \; a_3^2 - (a_3^2/c_3^2)(z-\ell_3)^2, & z_1 \leq z \leq z_2 \;\; : \;\; \rho\partial_z\rho = -(a_3^2/c_3^2)(z-\ell_3) \;, \\ R: \; a_2^2 - (a_2^2/c_2^2)(z-\ell_2)^2, & z_2 \leq z \leq z_3 \;\; : \;\; \rho\partial_z\rho = -(a_2^2/c_2^2)(z-\ell_2) \;. \end{cases} \tag{3-2}$$

where $z_0 \equiv \ell_1 - c_1$ and $z_3 \equiv \ell_2 + c_2$. Whereas the left and right shapes are always spheroids and thus have $a_i^2 > 0$ and $a_i^2/c_i^2 > 0$ for $i = 1, 2$, the corresponding quantities for the middle shape may have either sign. When $a_3^2/c_3^2 < 0$ the middle shape is either a hyperboloid of one sheet ($a_3^2 > 0$), or a hyperboloid of two sheets ($a_3^2 < 0$). We are not concerned with disconnected shapes here, but we note that shapes with $a_3^2/c_3^2 > 0$ and $a_3^2 < 0$ may occur for fairly compact shapes, so both a_3^2 and c_3^2 can have either sign for the family of connected 3QS shapes.

There are three parameters (a_i, c_i, ℓ_i) for each of the three sections, in addition to z_1 and z_2, but these are not independent: the middle sections must join the two end sections smoothly (at z_1 and z_2) and the nuclear volume must remain constant as its shape is changed. Nix introduced the following independent parameters [6]. The overall volume is governed by the length scale u given by $2u^2 = a_1^2 + a_2^2$, while the shape itself is described by six dimensionless parameters, three symmetric (σ_1, σ_2, σ_3) and three asymmetric (α_1, α_2, α_3),

$$\sigma_1 \;=\; \frac{\ell_2 - \ell_1}{u} \;,\;\; \sigma_2 = \frac{a_3^2}{c_3^2} \;,\;\; \sigma_3 = \tfrac{1}{2}\left(\frac{a_1^2}{c_1^2} + \frac{a_2^2}{c_2^2}\right) = \tfrac{1}{2}\left[\left(\frac{3-2\varepsilon_{\rm f1}}{3+\varepsilon_{\rm f1}}\right)^2 + \left(\frac{3-2\varepsilon_{\rm f2}}{3+\varepsilon_{\rm f2}}\right)^2 \right], \tag{3-3}$$

$$\alpha_1 \;=\; \frac{\ell_2 + \ell_1}{2u} \;,\;\; \alpha_2 = \frac{a_1^2 - a_2^2}{u^2} \;,\;\; \alpha_3 = \frac{a_1^2}{c_1^2} - \frac{a_2^2}{c_2^2} = \left[\left(\frac{3-2\varepsilon_{\rm f1}}{3+\varepsilon_{\rm f1}}\right)^2 - \left(\frac{3-2\varepsilon_{\rm f2}}{3+\varepsilon_{\rm f2}}\right)^2 \right], \tag{3-4}$$

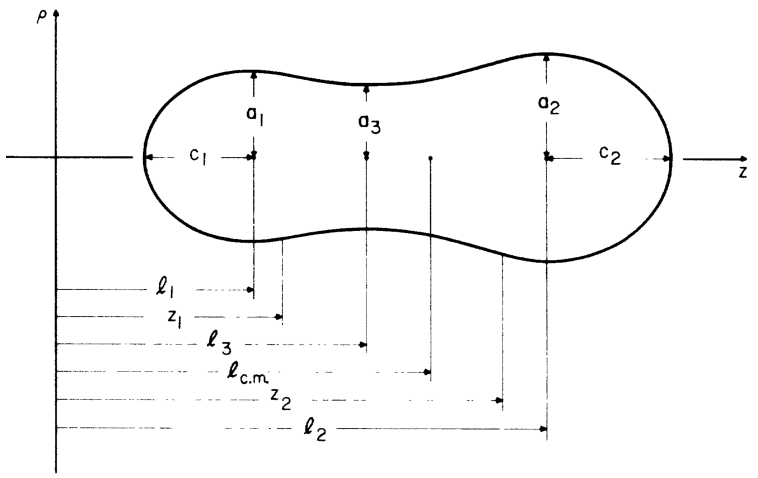

Figure 3-1: The three-quadratic-surfaces shape family for mononuclei: The left and right parts are pieces of spheroids with major and minor axes $c_{1,2}$ and $a_{1,2}$, centered at $\ell_{1,2}$; they are joined smoothly to the middle section which is part of either an ellipsoid or (shown) a hyperboloid of revolution. [From [6].]

where the relationships between the shape parameters σ_3 and α_3 and the ε deformations of the two spheroids are indicated for σ_3 and α_3. The addition of a common amount $\Delta\ell$ to the three parameters $\{\ell_i\}$ results merely in an overall translation of the systemby $\Delta\ell$ along the symmetry axis without any genuine shape change. Because the overall center of mass remains constant during the shape evolution, there are only five independent ways that the shape can change, *i.e.* the 3QS shape family is five-dimensional. One may think of these five shape degrees of freedom as representing the following qualitatively distinct characteristics:

1. the overall elongation (which qualitatively corresponds to the quadrupole moment of the nucleus, Q_2;
2. the degree of central bulging or indentation (for compact shapes this qualitatively corresponds to the hexadecapole moment Q_4, while it corresponds to the neck radius c for shapes near scission);
3. the degree of deformation of the left spheroidal end part (described by the value of $\varepsilon_{\rm f1}$);
4. the degree of deformation of the right spheroidal end part (described by the value of $\varepsilon_{\rm f2}$);
5. and the degree of reflection asymmetry (corresponding qualitatively to the octupole moment Q_3), often called the mass asymmetry.

These various shape degrees of freedom are expected to be the minimum required for an adequate description of fission.

4 Potential energy

Studies of fission dynamics need to consider systems that have a finite temperature, $T > 0$ (see Sect. 2.1), but for the time being T is taken to be zero, so the potential energy $U(\boldsymbol{q})$

is the energy of the lowest possible configuration of the nuclear system having the specified shape $\boldsymbol{q}$. It might seem desirable to calculate $U(\boldsymbol{q})$ on the basis of a purely microscopic many-body model. However, such approaches are generally computationally quite demanding and therefore somewhat impractical (millions of different shapes need to be treated for each nucleus considered, amplifying the computational burden very significantly). Moreover, it is generally somewhat difficult to obtain the absolute energy with good accuracy because of the complicated many-body interactions, though steady progess is being made. It is also somewhat complicated to impose the specified shape within a microscopic treatment.

The *macroscopic-microscopic* method presents a relatively easy alternative calculational approach that takes advantage of a characteristic feature of nuclear properties that is well brought out for nuclear masses: There is an overall smooth trend overlaid by relatively small undulatory deviations from the average. The central idea is therefore to write the potential energy of a nuclear system as a sum of a smooth term, $E_{\rm macro}(Z,N,{\rm shape})$, and a fluctuating correction term, $E_{\rm s+p}(Z,N,{\rm shape})$, that reflects the shell and pairing effects associated with the particular level scheme at the specified shape,

$$U(Z,N,{\rm shape}) \;=\; E_{\rm macro}(Z,N,{\rm shape}) \;+\; E_{\rm s+p}(Z,N,{\rm shape})\;. \tag{4-5}$$

The two terms will be discussed separately below. The above decomposition is useful for general shapes, whereas for masses it is often practical to use the macroscopic sphere as a reference,

$$U(Z,N,{\rm shape}) \;=\; E_{\rm macro}(Z,N,{\rm sphere}) \;+\; E_{\rm micro}(Z,N,{\rm shape})\;, \tag{4-6}$$

because $E_{\rm micro}({\rm shape}) = E_{\rm s+p}({\rm shape}) + E_{\rm macro}({\rm shape}) - E_{\rm macro}({\rm sphere})$ then represents *all* effects over and above the spherical macroscopic energy (which would have been the ground-state energy in the absence of structure effects). A concise introduction to the method was given in Ref. [7].

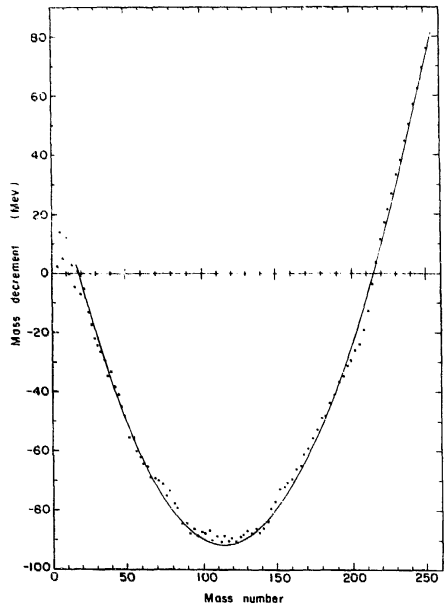

Figure 4-2: The nuclear mass defect versus the nuclear mass number A for 97 β-stable nuclei throughout the periodic table, as either (scattered dots) measured experimentally or (smooth solid curve) given by the nuclear liquid-drop model (see Sect. 4.1). The overall trend is globally well reproduced, also in the light region, and the differences represent the microscopic effects for individual nuclei (see Eq. (4-6)). (From Ref. [8].)

4.1 Macroscopic energy

In its simplest form, the expression for the macroscopic energy is based on the similarity between an atomic nucleus and a charged liquid drop [9, 10],

$$E_{\rm macro} = E_{\rm vol} + E_{\rm surf} + E_{\rm coul} + E_{\rm pair} \ . \tag{4-7}$$

The volume term is proportional to A and depends on the neutron-proton asymmetry through a factor of the form $1-\kappa[(N-Z)/A]^2$, the surface term is proportional to $A^{2/3}$, the Coulomb term ($\sim Z^2/A^{1/3}$) is the electrostatic repulsion between the protons, and the pairing term takes account of the increased binding when the number of protons and/or neutrons is even.

For fission, the most important macroscopic terms are the surface energy and the Coulomb energy which behave oppositely as the nucleus is deformed away from a sphere. A spheroid of eccentricity e has $E_{\rm surf}(e) \approx E_{\rm surf}(0)[1+\frac{2}{45}e^4]$ and $E_{\rm coul}(e) \approx E_{\rm coul}(0)[1-\frac{1}{45}e^4]$, so there will be a macroscopic fission barrier as long as $E_{\rm coul}(0) < 2E_{\rm surf}(0)$, which is the case up to $Z \approx 126$.

A succession of refinements have been made over the years. We sketch here the *finite-range liquid-drop* (FRLD) model [11, 12] which is being employed in modern calculations. The finite range of the nuclear interaction is taken into account by a phenomenological method motivated by the following considerations [13]:

1. For spherical configurations and large nuclei, the model should give roughly the same result as the standard liquid-drop model;

2. The model should be less sensitive to high-multipole ripples on the nuclear surface;

3. Between two separated nuclei there should be, in addition to the Coulomb repulsion, an attractive nuclear interaction, known as the *proximity* potential [14];

4. The model should be applicable to general shapes with reasonable computational effort.

The FRLD model describes the nuclear shape in terms of sharp generating distributions, $\hat\rho(\boldsymbol{r})$, which are unity inside the specified shape and zero outside. The nuclear surface energy is then obtained by use of a suitable smearing kernel $g(r)$, such as a Yukawa function [13],

$$E_S(\boldsymbol{\chi}) \ \sim \ V_0 - \int_{V(\boldsymbol{\chi})} g(|\boldsymbol{r}-\boldsymbol{r}'|)\, d^3\boldsymbol{r}\, d^3\boldsymbol{r}' \ , \quad g(r) = \frac{1}{4\pi a^3}\frac{{\rm e}^{-r/a}}{r/a} \ . \tag{4-8}$$

The range of the kernel $g(r)$ should account both for the finite range of the nucleon-nucleon interaction and the finite diffuseness of the nuclear matter distribution. Because the Yukawa function does not saturate, it is preferable to use a slightly more complicated kernel (a Yukawa plus an exponential) that leads to a surface energy with many desirable properties [15]. Such a kernel is used in the explicit expressions on the next page. The shape-dependent Coulomb energy is crrected for the diffuseness of the proton distribution by use of a similar kernel [16].

Once the macroscopic energy has been obtained, the microscopic theory is left with the much simpler task of evaluating only that part of the total binding energy that fluctuates due to the irregularities in the single-particle energy levels.

Finite-Range Liquid-Drop Model

$$
\begin{aligned}
&E_{\rm macro}(Z,N,{\rm shape}) \;= && (4\text{-}9)\\
&M_{\rm H}Z + M_{\rm n}N && \text{mass excesses of } Z \text{ hydrogen atoms and } N \text{ neutrons}\\
&-a_{\rm v}(1-\kappa_{\rm v}I^2)A && \text{volume energy}\\
&+a_{\rm s}(1-\kappa_{\rm s}I^2)B_1({\rm shape})A^{2/3} && \text{surface energy}\\
&+a_0A^0 && A^0 \text{ energy}\\
&+c_1Z^2/A^{1/3}\,B_3({\rm shape}) && \text{Coulomb energy}\\
&-c_4Z^{4/3}/A^{1/3} && \text{Coulomb exchange correction}\\
&+f(k_{\rm F}r_{\rm p})\,Z^2/A && \text{proton form–factor correction to Coulomb energy}\\
&-c_{\rm a}(N-Z) && \text{charge–asymmetry energy}\\
&+W\left(|I|+\left\{\begin{array}{ll} 1/A, & Z=N \text{ odd}\\ 0\,, & \text{otherwise}\end{array}\right\}\right)\times B_{\rm W}({\rm shape}) && \text{Wigner energy}\\
&+\left\{\begin{array}{ll} \overline{\Delta}_{\rm p}+\overline{\Delta}_{\rm n}-\delta_{\rm np}, & Z \text{ and } N \text{ odd}\\ \overline{\Delta}_{\rm p}\,, & Z \text{ odd, } N \text{ even}\\ \overline{\Delta}_{\rm n}\,, & Z \text{ even, } N \text{ odd}\\ 0\,, & Z \text{ and } N \text{ even}\end{array}\right\} && \text{average pairing energy}\\
&-a_{\rm el}Z^{2.39}\,. && \text{energy of } Z \text{ bound electrons}
\end{aligned}
$$

The relative neutron excess is $I=(N-Z)/(N+Z)=(N-Z)/A$. The Coulomb coefficients are

$$c_1 = \tfrac{3}{5}\frac{e^2}{r_0}\;,\;\; c_4 = \tfrac{5}{4}\left(\frac{3}{2\pi}\right)^{2/3} c_1\;,$$

while the function $f(k_Fr_{\rm p})$ in the proton form-factor correction to the Coulomb energy is

$$f(k_{\rm F}r_{\rm p}) = -\tfrac{1}{8}\frac{r_{\rm p}^2e^2}{r_0^3}\left[\frac{145}{48}-\frac{327}{2,880}(k_{\rm F}r_{\rm p})^2+\frac{1,527}{1,209,600}(k_{\rm F}r_{\rm p})^4\right]\;,\;\; k_{\rm F}=\left(\frac{9\pi Z}{4A}\right)^{1/3}\frac{1}{r_0}\;.$$

The average pairing gaps are $\overline{\Delta}_{\rm n} = r_{\rm mac}B_{\rm s}/N^{1/3}$ and $\overline{\Delta}_{\rm p} = r_{\rm mac}B_{\rm s}/Z^{1/3}$ and $\delta_{\rm np} = h/B_{\rm s}A^{2/3}$. Furthermore, $B_{\rm s}$ is the area of the surface S of the specified shape, relative to that of a sphere,

$$B_{\rm s}({\rm shape}) \;=\; \frac{1}{4\pi R_0^2}\oint dS\;,\;\; R_0 = r_0A^{1/3}\;,$$

while B_1 is the relative effective surface area due to the finite range,

$$B_1({\rm shape}) \;=\; \frac{1}{8\pi^2R_0^2a^4}\int_V d^3\boldsymbol{r}\int_V d^3\boldsymbol{r}'\left(2-\frac{|\boldsymbol{r}-\boldsymbol{r}'|}{a}\right)\frac{{\rm e}^{-|\boldsymbol{r}-\boldsymbol{r}'|/a}}{|\boldsymbol{r}-\boldsymbol{r}'|/a}\;,$$

and B_3 is the relative Coulomb energy,

$$B_3({\rm shape}) \;=\; \frac{15}{32\pi^2R_0^5}\int_V d^3\boldsymbol{r}\int_V d^3\boldsymbol{r}'\frac{1}{|\boldsymbol{r}-\boldsymbol{r}'|}\left[1-\left(1+\tfrac{1}{2}\frac{|\boldsymbol{r}-\boldsymbol{r}'|}{a_{\rm den}}\right){\rm e}^{-|\boldsymbol{r}-\boldsymbol{r}'|/a_{\rm den}}\right]\;,$$

where V denotes the volume enclosed by the specified shape. More details are given in Ref. [11].

4.2 Shell-plus-pairing energy

The shell-plus-pairing energy in (4-5) is the sum of separate contributions from neutrons and protons which can be obtained from the respective single-particle levels $\{\epsilon^{\rm n}_\nu\}$ and $\{\epsilon^{\rm p}_\nu\}$. These are obtained by solving the Schrödinger equation,

$$\left[-\frac{\hbar^2}{2m}\Delta + V^{\rm n,p}(\boldsymbol{r})\right]\psi^{\rm n,p}_\nu(\boldsymbol{r}) = \epsilon^{\rm n,p}_\nu\,\psi^{\rm n,p}_\nu(\boldsymbol{r})\ , \tag{4-10}$$

where $\Delta = \boldsymbol{\nabla}^2 = \partial^2/\partial\boldsymbol{r}^2$ is the Laplace operator, in the effective single-particle potential,

$$V^{\rm n,p}(\boldsymbol{r}) = V^{\rm n,p}_{\rm mf}(\boldsymbol{r}) + V^{\rm n,p}_{\rm so}(\boldsymbol{r}) + V^{\rm n,p}_{\rm C}(\boldsymbol{r})\ . \tag{4-11}$$

The mean-field, the spin-orbit, and the Coulomb terms for neutrons and protons are given by

$$\text{Mean field:}\qquad V^{\rm n,p}_{\rm mf}(\boldsymbol{r}) = -V^{\rm n,p}_0\int_\Omega g(|\boldsymbol{r}'-\boldsymbol{r}|)\,d^3\boldsymbol{r}'\ ,\ \ g(r) = \frac{1}{4\pi a^3}\frac{{\rm e}^{-r/a}}{r/a}\ , \tag{4-12}$$

$$\text{Spin}-\text{orbit:}\qquad V^{\rm n,p}_{\rm so}(\boldsymbol{r}) = i\lambda\left(\frac{\hbar}{2mc}\right)^2\boldsymbol{\sigma}\cdot\frac{\partial V^{\rm n,p}_{\rm mf}(\boldsymbol{r})}{\partial\boldsymbol{r}}\times\frac{\partial}{\partial\boldsymbol{r}}\ , \tag{4-13}$$

$$\text{Coulomb:}\qquad V^{\rm p}_{\rm C}(\boldsymbol{r}) = \frac{Ze^2}{\frac{4}{3}\pi R_0^3}\int_\Omega\frac{d^3\boldsymbol{r}'}{|\boldsymbol{r}'-\boldsymbol{r}|}\ +\text{finite}-\text{range corr.}\ ,\ V^{\rm n}_{\rm C}(\boldsymbol{r}) = 0\,. \tag{4-14}$$

The single-particle level schemes depend on the nuclear shape. The level distribution is usually irregular and may exhibit significant gaps for particular shapes, often associated with special geometrical symmetries, as illustrated in Fig. 4-3.

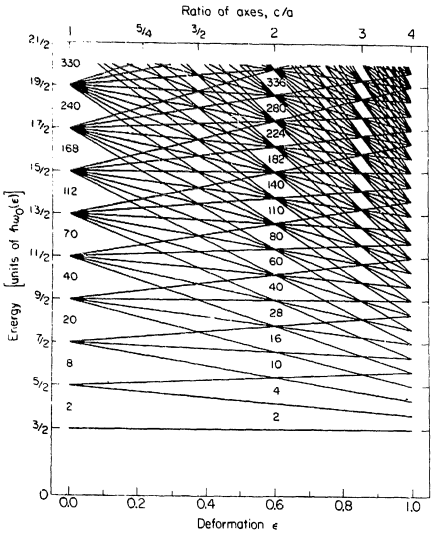

Figure 4-3: Energy levels in a three-dimensional harmonic-oscillator potential well as functions of its spheroidal deformation. When the potential is spherically symmetric, the associated large degree of degeneracy causes the energy levels to bunch,leading to clearly defined major shells. As the potential deforms, some orbitals fit better into the spheroidal cavity (namely those with motion predominantly along the symmetry axis) and their energies decrease, while the energy increases for orbitals that have predominantly transverse motion; this leads to a steady erosion of the shell structure. However, when the axis ratio attains a simple value (2:1, 3:1, ...) some degree of degeneracy is reestablished and new shell structures arise. (From Ref. [7].)

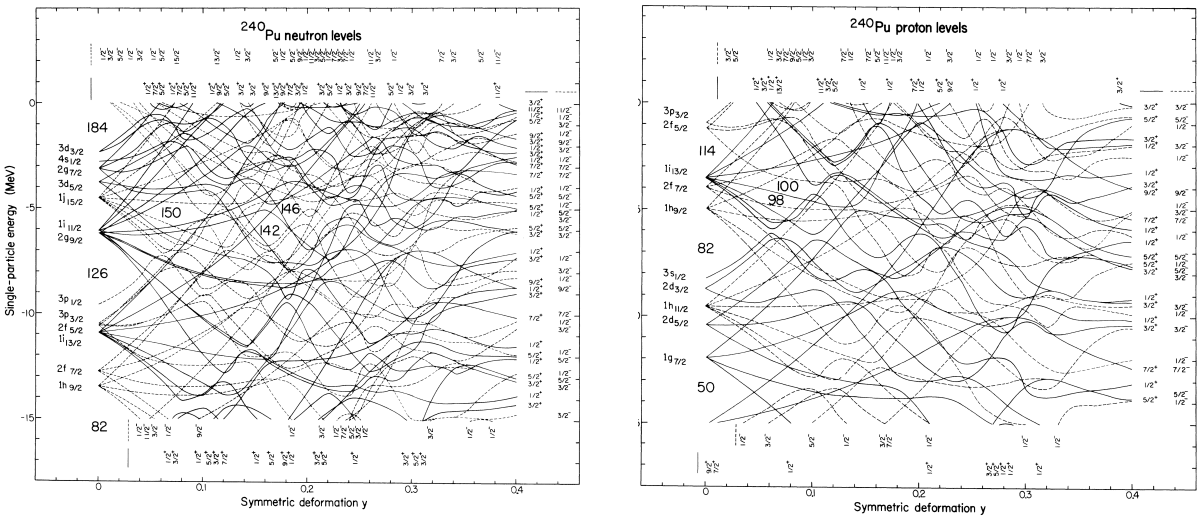

Figure 4-4: Neutron (*left*) and proton (*right*) level diagrams (often called Nilsson diagrams) for ^{240}Pu: The single-particle energies plotted as functions of the (reflection-symmetric) distortion. [From Ref. [17].]

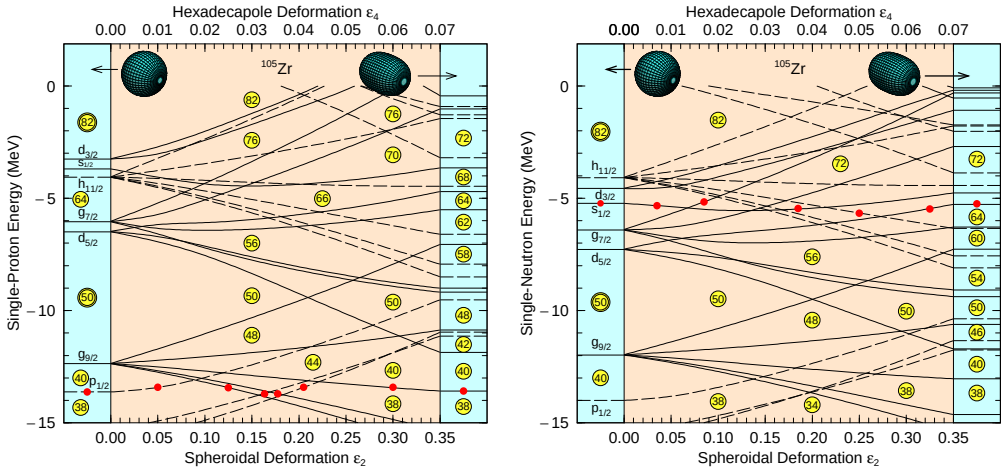

Figure 4-5: Neutron (*left*) and proton (*right*) level diagrams for ^{105}Zr: The single-particle energies plotted as functions of the (reflection-symmetric) distortion. [From Ref. [18].]

4.2 Shell effects

A simple quantitative metod for obtaining the shell energy was proposed by Myers and Swiatecki [8] and further developed by Strutinsky [19]; it was further discussed in Ref. [20]. The method is briefly outlined below for neutrons or protons. 4-a

The actual density of single-particle states is discrete, $g_0(\epsilon) = \sum_\nu \mathsf{g}_\nu \delta(\epsilon - \epsilon_\nu)$, where g_ν is the degeneracy of the level ν. [It is common to refer to the density of states as the "level density", even though it is incorrect (unless no levels are degenerate, $\mathsf{g}_\nu = 1$).] A corresponding smooth density of states is obtained by averaging (or smearing) the actual single-particle level density over an appropriate energy region,

$$\tilde{g}(\epsilon) \;=\; \frac{1}{\gamma}\int_{-\infty}^{+\infty} \xi\left(\frac{\epsilon-\epsilon'}{\gamma}\right) g_0(\epsilon')\, d\epsilon' \tag{4-15}$$

where $\xi(\epsilon/\gamma)$ is a suitable smearing function with an adjustable range γ. The Fermi energy λ for neutrons or protons is determined by number conservation,

$$\int_{-\infty}^{\lambda} \tilde{g}(\epsilon)\, d\epsilon \;\doteq\; N \text{ or } Z\ . \tag{4-16}$$

The shell energy for neutrons or protons is then given by

$$\delta E_{\rm shell} \;=\; \int_{-\infty}^{\lambda} g_0(\epsilon)\,\epsilon\, d\epsilon - \int_{-\infty}^{\lambda} \tilde{g}(\epsilon)\,\epsilon\, d\epsilon \;=\; \sum_{\epsilon_\nu<\lambda} \mathsf{g}_\nu\epsilon_\nu - \int_{-\infty}^{\lambda} \tilde{g}(\epsilon)\,\epsilon\, d\epsilon\ . \tag{4-17}$$

Figure 4-6 shows the function $\delta E^{\rm n}_{\rm shell}(\lambda)$ for ^{208}Pb:

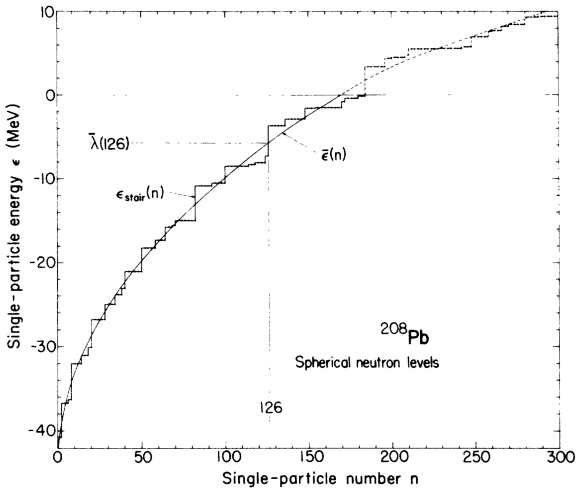

Figure 4-6: For the neutron levels in ^{208}Pb at a spherical shape are shown the accumulated sum of the eigenvalues and the corresponding smooth quantity, both given in Eq. (4-17). The shell correction for the neutrons is the difference between those two quantities. (From Ref. [17].)

In nuclear fission, a compact mononucleus develops gradually into two separate nuclear fragments. It is a significant advantage of the Strutinsky method that when the system has acquired a distinct binary character, the extracted shell energy will reflect the level structure in the individual fragments even though the calculation is done for the single-particle field associated with the combined dinuclear system. 4-b

4.2 Pairing

The nuclear pairing force plays an important role for nuclear properties at low energy, such as binding energies, β-strength functions, and quasi-particle energies. In the macroscopic-microscopic approach to nuclear energies, one needs the difference between the pairing correlation energy associated with the actual single-particle states and that of the corresponding average state density $\tilde{g}(\epsilon)$ (the same one used above to obtain the shell correction energy),

$$\delta E_{\rm pair} \;=\; E_{\rm pair}[g_0] \;-\; \tilde{E}_{\rm pair}[\tilde{g}] \;. \tag{4-18}$$

for neutrons and protons separately. A variety of models have been employed for the calculation of the pairing correlation energy [21, 22].

The simplest and most widely employed treatment of pairing is the Bardeen-Cooper-Schrieffer (BCS) model. In a suitable region around the Fermi surface, $\nu_1 \le \nu \le \nu_2$, it replaces the particles by quasi-particles whose energies are given by

$$E_\nu \;=\; \Big[(\epsilon_\nu - \lambda)^2 + \Delta^2\Big]^{1/2} \;, \tag{4-19}$$

and the probability that a particle state is occupied is given by $v_\nu^2 = \frac{1}{2}\,[1 - (\epsilon_\nu - \lambda)/E_\nu]$. The pairing gap $\Delta_{\rm n,p}$ and the Fermi energy $\lambda_{\rm n,p}$ are determined from the two coupled equations,

$$N \text{ or } Z \;\doteq\; 2(\nu_1 - 1) + 2\sum_{\nu=\nu_1}^{\nu_2} v_\nu^2 \;, \quad \frac{2}{G} \;\doteq\; \sum_\nu \frac{1}{E_\nu} \;, \tag{4-20}$$

where $G_{\rm n,p}$ is the pairing interaction strength for neutrons or protons and double degenerary is assumed, $\mathsf{g}_\nu = 2$. The pairing correlation energy for neutrons or protons is then given by

$$E_{\rm pair} \;=\; \sum_\nu [2v_\nu^2 - n_\nu]\,\epsilon_\nu - \frac{\Delta^2}{G} - \tfrac{1}{2}G\sum_{\nu=\nu_1}^{\nu_2}[2v_\nu^4 - n_\nu] + E_\nu\,\theta_{\rm odd}^{N,Z} \;, \tag{4-21}$$

where $n_\nu = 0, 1, 2$ are the occupancies of the doubly degenerate levels in the absence of pairing and the last term is unity/zero if the number of neutrons or protons is odd/even.

Because the simple BCS model fails for large level spacings, it is sometimes replaced by the Lipkin-Nogami approximation. At present [11], the macroscopic-microscopic calculations of nuclear potential energies employ this refinement of the BCS model, which takes account of the lowest-order correction to the total energy arising from the fluctuations in particle number.

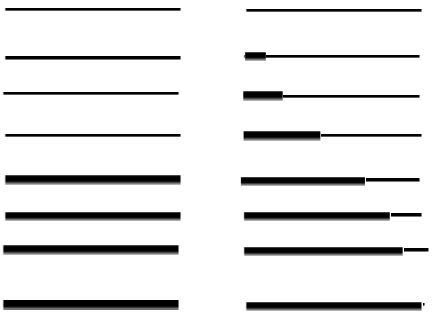

Figure 4-7: Illustration of the BCS pairing treatment: Without paring (*left*), the single-particle states are fully occupied below the Fermi surface ($\epsilon_\nu < \lambda$) and empty above it ($\epsilon_\nu > \lambda$); the pairing interaction causes the states around the Fermi surface to become partially occupied with the probability v_ν^2 (*right*). The pairing correction to the nuclear energy is the difference between the pairing energy for the actual level distribution and that for the corresponding constant level density.

4.3 Calculated results

The macroscopic-microscopic method has been used extensively for many years and has provided quantatively useful results for a variety of nuclear properties, as very briefly illustrated below.

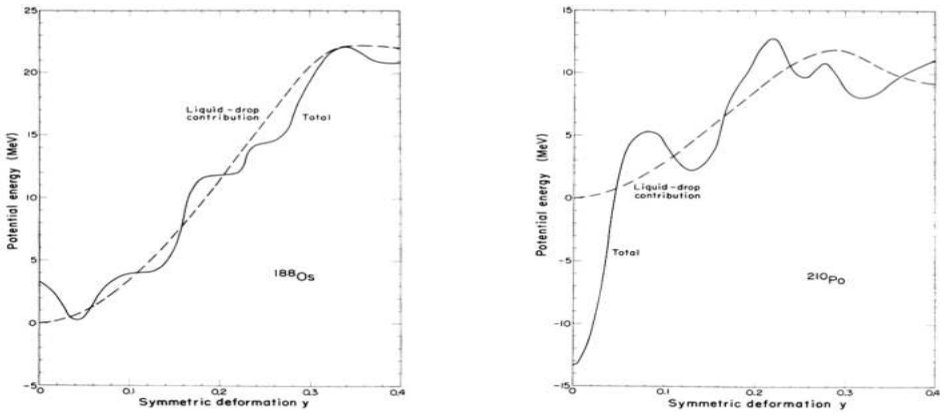

Figure 4-8: Approximate fission barriers for ^{188}Os and ^{210}Po: the potential energy along a preselected sequence of ever more elongated shapes having reflection and axially symmetry. Both the total potential (solid) and the macroscopic part (dashed) are plotted. For osmium the macroscopic barrier is so high that the undulating microscopic corrections do not produce any additional extrema, whereas several appear for polonium. For osmium $E_{\rm s+p}$ is positive for the spherical shape so the ground state is deformed, but the total microscopic contribution to the ground-state mass is small; for polonium $E_{\rm s+p}$ is strongly negative for a sphere so the ground state is spherical and has $E_{\rm micro} = E_{\rm s+p}$. (From [17].)

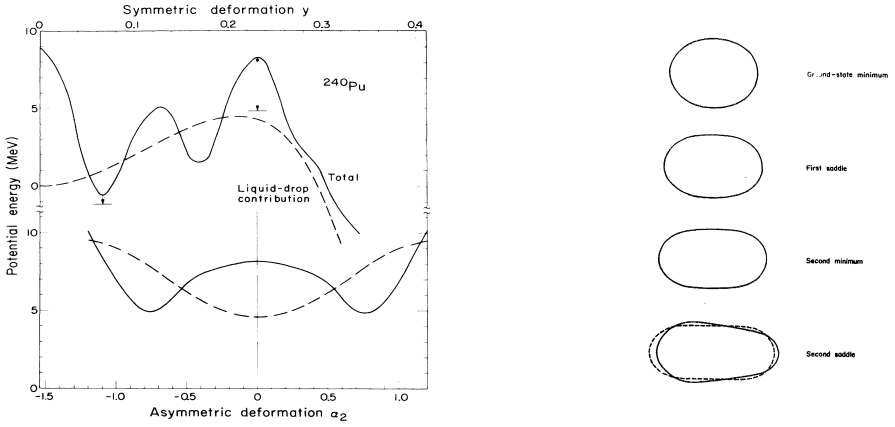

Figure 4-9: The fission barrier for ^{240}Pu: *Left:* The lowest potential energy as a function of the degree of reflection-symmetric elongation (*top*) and the energy of the saddle point for a specified degree of reflection asymmetry (*bottom*); both the total potential (solid) and the macroscopic part (dashed) are plotted. *Right:* The nuclear shape at various stationary points in potential-energy landscape: the first minimum, the first saddle, the second minimum, and the second saddle; the latter is symmetric if only the macroscopic energy is considered (dashed), while the addition of the microscopic correction renders it asymmetric (solid). (From [17].)

The macroscopic-microscopic method has been particularly useful for making global calculations of nuclear masses. Within a suitable shape parametrization, the lowest potential-energy minimum is located and identified with the nuclear ground state, for which the properties can then be extracted, such as the shape and the binding energy.

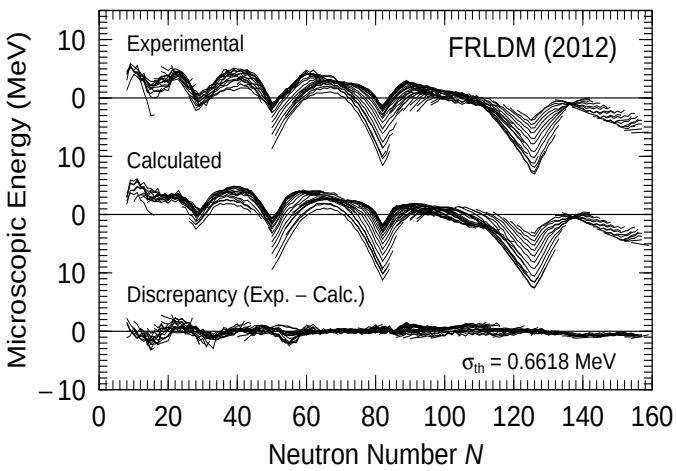

Figure 4-10: As a function of the neutron number N are shown the microscopic part of the nuclear mass defects (which exhibit significant shell structure) as obtained from experiment (*top*); as calculated by the macroscopic-microscopic method [11] (*middle*), which yields a globally very good reproduction of the data; and the discrepancies (*bottom*) which are about 0.67 MeV on average (recent model enhancements have reduced the mean discrepancy to ≈0.56 MeV). (From Ref. [11].)

The ability to calculate the nuclear potential energy for arbitrary shapes is of key importance for fission studies. The most basic features of interest are minima and saddles.

Figure 4-11: An early depiction of the potential-energy landscape for ^{236}U in a two-dimensional representation using a combination of ε_2 and ε_4 distortions for the elongation and a combination of ε_3 an and ε_5 distortions for the mass asymmetry [23], as seen either from above (*left*) or at an angle (*right*). The ground-state minimum is located on the left and the isomeric minimum is near the center; both are reflection symmetric and they are separated by the (also symmetric) first saddle. By contrast, the second saddle (on the right) is asymmetric and has an energy significantly below the conditional symmetric barrier (the mountain top on the right).

In order to adequately describe the shapes explored by the fissioning nucleus, a sufficient number of shape degrees of freedom are required (see Sect. 3). A five-dimensional tabulation has been made of the potential-energy for more than five thousand nuclei [12]:

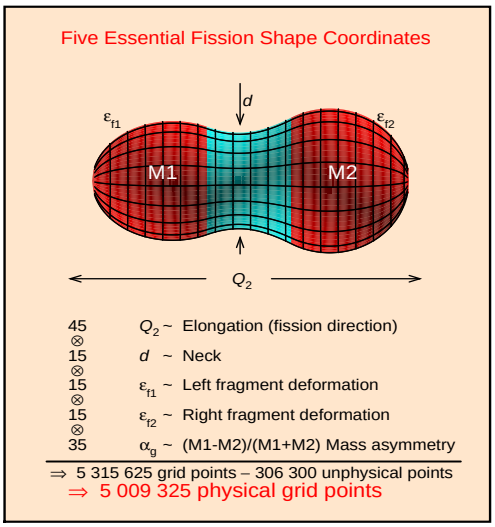

Figure 4-12: The five-dimensional lattice in the space of the center-of-mass conserving shape parameters for the three-quadratic-surface family [6] introduced by P. Möller for the tabulation of macroscopic-microscopic potential-energy surfaces [12]. Each shape is characterized by five integers $(IJKLM)$ which respectively govern the overall quadrupole moment Q_2, the neck radius d, the left and right spheroidal deformations ϵ_{f1} and ϵ_{f2}, and the reflection asymmetry α_g. The lattice thus contains more than five million different shapes, in addition to a number of shapes. (From Ref. [24] as extended by Peter Möller.)

The potential-energy landscape may provide considerable insight into the fission process. For example (as illustrated below in Fig. 4-13), it may be readily possible to anticipate whether a particular system will fission symmetrically or not:

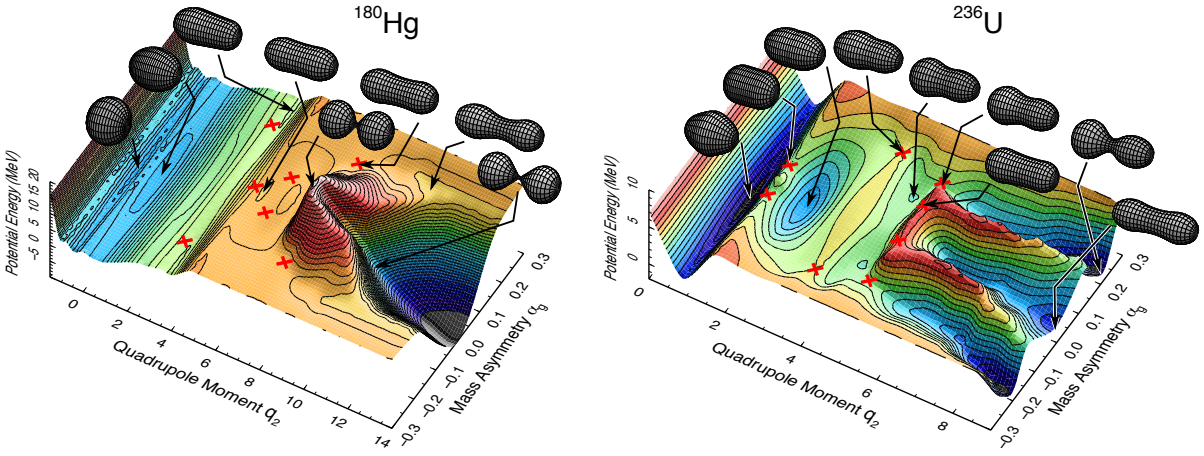

Figure 4-13: The 5D potential energy surface for ^{180}Hg and ^{236}U reduced to a two-dimensional landscape presenting some of its major features. There are important qualitative differences between the two cases: ^{236}U displays a strong preference for a certain mass asymmetry and the associated valley develops rather early; for ^{180}Hg symmetric fission is blocked even more at small Q_2, but at larger Q_2 the landscape shows no preference for any particular asymmetric split. One would then expect that the calculated fragment mass distribution for ^{180}Hg will show a larger sensitivity than ^{236}U to the structure of the dissipation tensor and possibly to that of the inertial-mass tensor as well. (From Ref. [25].)

5 Inertial mass

The inertial mass associated with nuclear shape changes is still far from being well understood and it is yet not possible to calculate inertial-mass tensors with an accuracy even remotely approching that with which the potential can be obtained. Furthermore, while microscopic studies have yielded valuable insight, such approaches tend to be very cumbersome and they have not yet been carried out for the large number of shapes required for fission dynamics.

It has therefore been common to resort to simple fluid-dynamical considerations (even though those may not be appropriate for nuclear shape dynamics at low energy where the nucleonic mean free path is relatively long and, in addition, there may be special effects from pairing correlations and shell structure). The kinetic energy is then given by

$$K(\boldsymbol{q},\dot{\boldsymbol{q}}) = \tfrac{1}{2}m\int \rho(\boldsymbol{r})\,\boldsymbol{v}(\boldsymbol{r})^2\,d^3\boldsymbol{r} = \tfrac{1}{2}m\rho_0\int_{z_{\rm min}}^{z_{\rm max}} dz \int_0^{\rho(z)} 2\pi\rho d\rho\,[v_\perp(\rho,z)^2 + v_\parallel(\rho,z)^2]\ , \qquad (5\text{-}1)$$

where $v_\parallel(\rho,z)$ is the longitudinal component of the local flow velocity $\boldsymbol{v}(\boldsymbol{r})$ and $v_\perp(\rho,z)$ is its transverse component. It is generally assumed that the nuclear flow is incompressible and irrotational. As a further simplification, one often invokes the Werner-Wheeler approximation which assumes that the fluid within a given transverse slice of the nucleus remains in that slice as the shape changes (see Fig. 5-1). Then the longitudinal flow velocity of a given fluid element does not depend on its distance ρ from the symmetry axis, $v_\parallel(\rho,z) = v_\parallel(z)$, and the rate of local expansion, $v_\perp(\rho,z)$, is proportional to ρ. As a result, the kinetic energy of the collective flow is elementary to express in terms of the collective velocities $\{\dot{q}_i\}$ and the associated mass tensor elements $M_{ij}(\boldsymbol{q})$ can then be obtained. This has been done for the 3QS shapes by Nix [26, 27] (though the resulting expressions are rather involved).

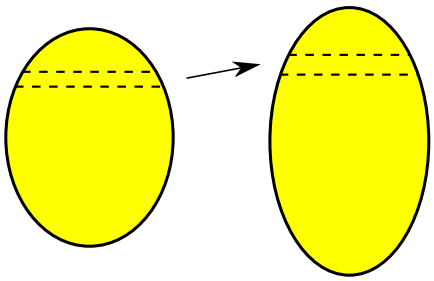

Figure 5-1: Illustration of the Werner-Wheeler approximation to incompressible and irrotational flow: The fluid remains within the same slice as the nuclear shape is changed. In the example shown, the slice moves upwards as the nucleus is stretched, its cross section becomes smaller, and it grows correspondingly wider, retaining its volume.

6 Dissipation

Because nucleons are fermions, an individual nucleon interacts with the remainder of the many-body system primarily through the effective one-body field (the "mean field"), at the relatively low energies of interest here. Furthermore, because of the leptodermous nature of nuclei, this interaction is concentrated in the surface region (where the density and hence the effective field vary most strongly). One may therefore expect that the dissipative coupling between the nuclear shape and the residual system can be understood by considering the interaction of the individual nucleons with the deforming one-body potential [28]. This type of dissipation is dominant for systems in which the constituents have a long mean-free path and it is called *one-body dissipation* because it can be derived on the basis on the effective one-body Hamiltonian that governs the nucleonic motion in the mean field. It may be contrasted with the more familiar fluid-dynamical dissipation (viscosity) which depends on the two-body interactions between the constituents. Expressions for the one-body dissipation tensor can be derived by elementary means for particularly simple nuclear geometries (Sects. 6.1 and 6.2).

One-body dissipation has two characteristic features that have important bearings on fission dynamics; both of them arise because the nucleons form a highly degenerate Fermi gas at the relatively low excitations of interest here:

1. Nuclear one-body dissipation is relatively *strong* because it is proportional to the mass density of the nucleons and their mean speed and the latter is of the order of the Fermi speed which is large compared to the typical surface motion;

2. Nuclear one-body dissipation is rather independent of the nuclear temperature because the nucleonic speeds in a degenerate Fermi gas do not increase much with temperature.

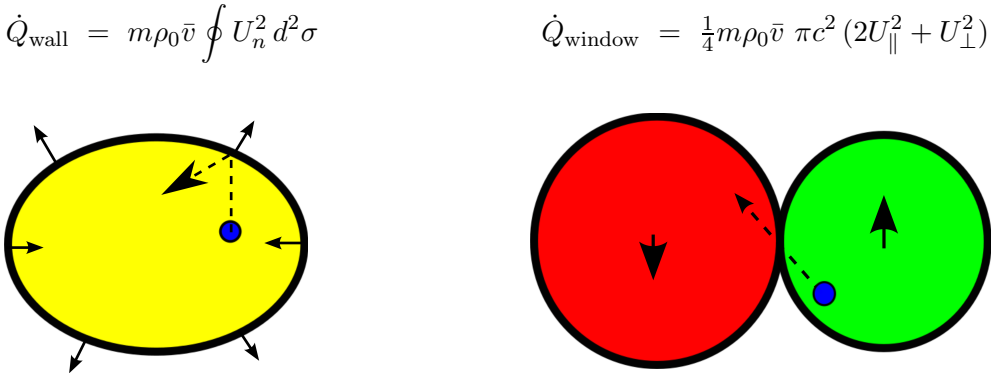

Figure 6-1: Illustration of the nuclear one-body dissipation mechanism: The *wall* dissipation acts when nucleons are reflected off the moving wall of a deforming incompressible vessel (*left*), while the *window* dissipation acts when nucleons transfer between two vessels in relative motion (*right*).

6.1 One-body dissipation in a mononucleus

The standard wall formula for one-body dissipation in a mononucleus is given by [28]

$$\dot{Q}^{\rm wall}(\boldsymbol{q},\dot{\boldsymbol{q}}) \;=\; m\rho_0\bar{v}\oint \dot{n}^2 d^2\sigma \;=\; \sum_{ij}\dot{q}_i\gamma_{ij}^{\rm wall}(\boldsymbol{q})\dot{q}_j \;, \tag{6-1}$$

where the integral is over the nuclear surface. Furthermore, m is the nucleon mass, ρ_0 is the bulk density of nucleons, and $\bar{v}$ is the mean speed of the nucleons in the bulk. For an axially symmetric surface defined by $\rho(z,t)$, the normal velocity of the local surface element is [29]

$$\dot{n} \;=\; \frac{\partial\rho}{\partial t}\Big/\left[1+\left(\frac{\partial\rho}{\partial z}\right)^2\right]^{1/2} \;=\; \sum_i \dot{q}_i\,\rho\frac{\partial\rho}{\partial z}\left[\rho^2+\left(\rho\frac{\partial\rho}{\partial z}\right)^2\right]^{-\frac{1}{2}} \;. \tag{6-2}$$

The elements of the wall dissipation tensor are then readily obtained,

$$\gamma_{ij}^{\rm wall}(\boldsymbol{q}) = 2\pi m\rho_0\bar{v}\int_{z_{\rm min}}^{z_{\rm max}}(\rho\frac{\partial\rho}{\partial q_i})(\rho\frac{\partial\rho}{\partial q_j})\left[\rho^2+(\rho\frac{\partial\rho}{\partial z})^2\right]^{-\frac{1}{2}}dz \;. \tag{6-3}$$

Sometimes the strength is considered to be adjustable, leading to a somewhat smaller value.

6.2 One-body dissipation in a dinucleus

As the fissioning nucleus approaches scission, its shape acquires a binary appearance and the system can be considered as a dinucleus joined by a relatively small neck though which individual nucleons may be exchanged. The associated dissipation rate is given by the *window* formula [28],

$$\dot{Q}^{\rm window} \;=\; \tfrac{1}{4}m\rho_0\bar{v}\,\pi c^2\,(2U_\parallel^2+U_\perp^2) \;=\; \sum_{ij}\dot{q}_i\gamma_{ij}^{\rm window}(\boldsymbol{q})\dot{q}_j \;, \tag{6-4}$$

where c is the radius of the neck (which is here assumed to have axial symmetry). Furthermore, $U_\parallel$ is the component of the relative dinuclear motion along the normal to the window and $\boldsymbol{U}_\perp$ is the component in the plane of the window. In addition, the shape changes of the two binary partners (the prefragments) give rise to two wall dissipation terms, each one with $\dot{n}$ calculated relative to the respective prefragment motion. The combined wall-plus-window dissipation is then described by [29],

$$\begin{aligned}\gamma_{ij}^{\rm w+w}(\boldsymbol{q}) \;&\equiv\; \gamma_{ij}^{\rm wall}(\boldsymbol{q})+\gamma_{ij}^{\rm window}(\boldsymbol{q}) \;=\; \tfrac{1}{2}m\rho_0\bar{v}\left\{\frac{\partial R}{\partial q_i}\frac{\partial R}{\partial q_j}\,\pi c^2\right. \\ &+\; \left.\pi\int_{z_0}^{z_3}dz\left(\frac{\partial\rho^2}{\partial q_i}-\tfrac{1}{2}\frac{\partial\rho^2}{\partial z}\frac{\partial R}{\partial q_i}\right)\left(\frac{\partial\rho^2}{\partial q_j}-\tfrac{1}{2}\frac{\partial\rho^2}{\partial z}\frac{\partial R}{\partial q_j}\right)\left[\rho^2+\tfrac{1}{4}\left(\frac{\partial\rho^2}{\partial z}\right)^2\right]^{-\frac{1}{2}}\right\} \;.\end{aligned} \tag{6-5}$$

6.3 Average macroscopic fission dynamics

The role played by the character of the dissipation can be illustrated by the most probable dynamical fission trajectories calculated macroscopically, *i.e.* wihout any microscopic corrections. Relative to non-dissipative dynamics ($\boldsymbol{\gamma}(\boldsymbol{q}) = \mathbf{0}$), the use of standard two-body viscosity of increasing strength causes the scission shapes to grow ever more elongated. The use of one-body dissipation has the opposite effect, leading to very compact (and slowly evolving) scission shapes.

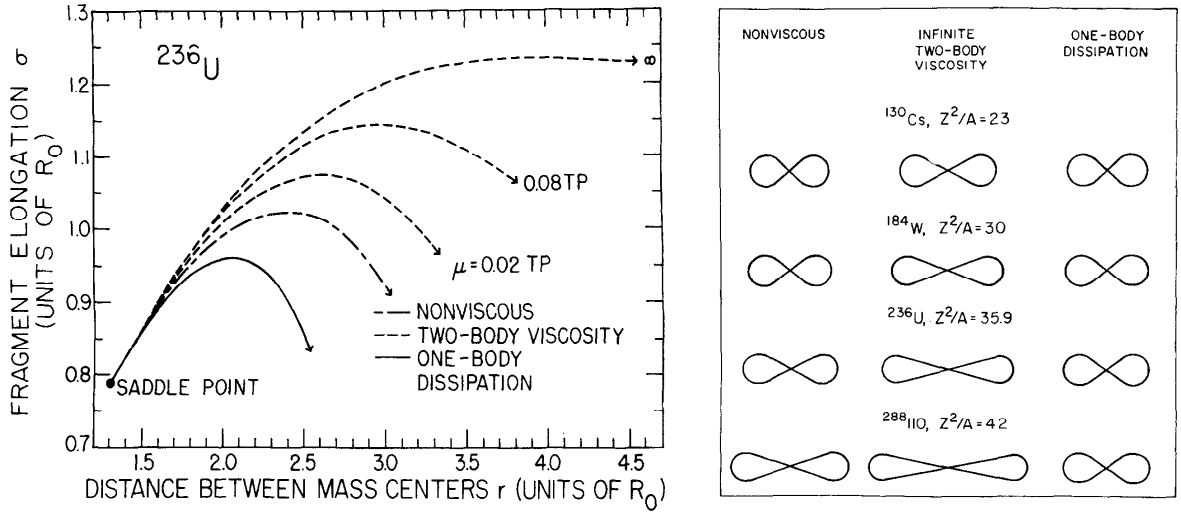

Figure 6-2: Effect of dissipation on the most probable macroscopic fission dynamics for ^{236}U (from Ref. [28]). *Left:* The average dynamical shape paths in the $r - \sigma$ plane (where r is the distance between the mass centers of the two halves and σ is the elongation of the (equal) fragments) from the macroscopic saddle point to scission, as calculated with either the standard one-body wall dissipation (solid curve) or two-body dissipation of various strengths ranging from 0 to ∞ (dashed curves). *Right:* The scission shapes for four nuclei with a range of fissilities Z^2/A as calculated for non-dissipative dynamics (*left*), infinite two-body viscosity (*center*), and the one-body wall dissipation given in Eq. 6-3 (*right*).

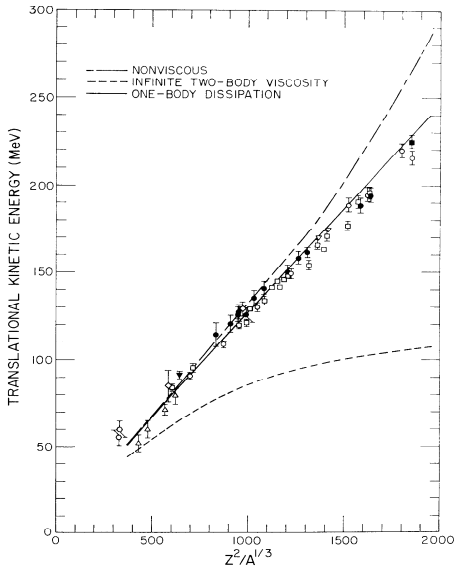

Figure 6-3: Comparison of calculated and measured (most probable) fission-fragment kinetic energies as functions of $Z^2/A^{1/3}$, calculated with either one-body dissipation (solid curve) or two-body viscosity with vanishing or infinite strength (dashed curves). The data are for cases in which the most probable division is symmetric (see Ref. [27]). The experimental kinetic energies can be reproduced by either adjusting the two-body viscosity, in which case the scission configurations are elongated but stretching relatively quickly, or by the one-body wall dissipation (6-3), in which case the scission configurations are compact but only slowly evolving. (From Ref. [28].)

7 Fission dynamics

In the preceding, we have described the various physical ingredients required for the calculation of the dynamical evolution of the nuclear shape. We discuss here a variety of aspects regarding the computational solution of the Langevin equation (2-9) for fission studies.

To study fission at thermal neutron energies, one would ideally sample the initial shape, $\boldsymbol{q}_0$, together with the corresponding momenta, $\boldsymbol{p}_0$, from the quasi-equilibrium distribution around the ground-state minimum and then calculate the time evolution, $\boldsymbol{q}(t)$, by propagating the shape with the Langevin equation until scission has occurred and the two fragments are well separated. This procedure would yield one fission event and it would need to be repeated until the sample of events obtained is sufficiently large to allow the extraction of the quantities of interest.

However, this naive procedure would not be computationally efficient because the system is likely to spend a long time roaming around the neighborhood of the ground-state minimum before accidentally stumbling across the first barrier and into the region of the second minimum, where again it is likely to spend a long time before either returning to the region around the first minimum og traversing the outer barrier and proceeding towards scission.

One may thus speed up the occurrence of fission, without affecting the extracted results, by starting the calculation at or near the second minimum and, furthermore, introducing some artificial way of discouraging the shape from "going backwards", *i.e.* from becoming more compact. Such a bias can be employed in a variety of ways. A more radical way of reducing the computational effort is to start the system near or slightly beyond the last barrier, but this has to be done with particular care to ensure that the results are reliable. While these issues are purely technical, it is practically essential to consider them.

Particularly important observables are the fission fragment mass A_f and the total kinetic energy K of the emerging fragments. The mass partition is essentially frozen in already before scission occurs, because further changes in the mass asymmetry are strongly hindered when the neck has become small. By contrast, the kinetic energy does not reach its final value until the fragments have separated beyond the reach of their mutual Coulomb repulsion (see Fig. 7-1). However, once the fragments have separated beyond the reach of the nuclear attraction, their asymptotic kinetic energy can be obtained by augmenting their current kinetic energy by their current mutual Coulomb potential energy (which is much larger).

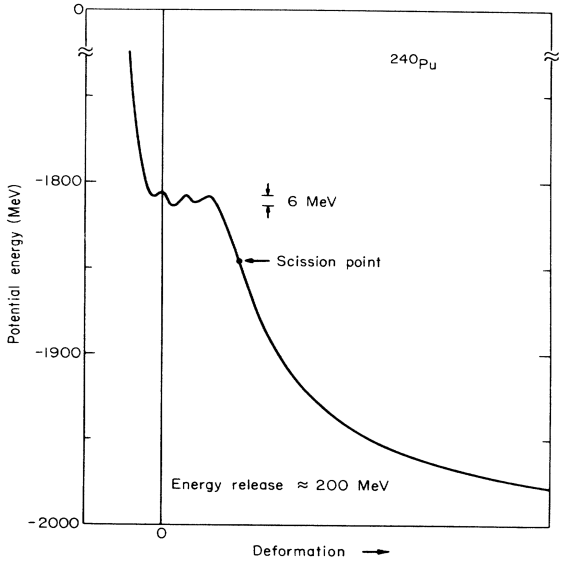

Figure 7-1: For the most probable division of ^{240}Pu is plotted the dependence of the potential energy of deformation on distance between the centers of the two parts of the system (divided according to the mass asymmetry degree of freedom). It should be noted that the energy changes prior to scission ($\approx$6 MeV) are rather small compared to the energy associated with the mutual Coulomb repulsion ($\approx$200 MeV). (From Ref. [17].)

7.1 Smoluchowski limit

As mentioned earlier (Sect. 6), the dissipation associated with the shape dynamics during fission is rather strong. If that is indeed the case then the inertial mass plays a less crucial role in the shape evolution and it may be possible to simplify the treatment, as explained below.

When the dissipation is very strong, then the velocities are small. One may then ignore all accelerations, $\ddot{q}_i \approx 0$, as well as terms of second order in the velocities, $\dot{q}_i\dot{q}_j \approx 0$. Therefore $\dot{p}_i = \sum_{jk}(\partial B_{ij}/\partial q_j)\dot{q}_k\dot{q}_j + \sum_j B_{ij}\ddot{q}_j \approx 0$ and the Langevin equation of motion (2-9) reduces to the *Smoluchowski* equation,

$$\boldsymbol{0} \;=\; \boldsymbol{F}^{\rm pot}(\boldsymbol{q}) + \boldsymbol{F}^{\rm fric}(\boldsymbol{q},\dot{\boldsymbol{q}}) + \boldsymbol{F}^{\rm ran}(\boldsymbol{q},t)\ . \tag{7-1}$$

Recalling that $\boldsymbol{F}^{\rm fric} = -\boldsymbol{\gamma}\cdot\dot{\boldsymbol{q}}$, we see that this equation is only of first order in time. We can therefore readily express the instantaneous velocity,

$$\dot{\boldsymbol{q}}(t) \;=\; \boldsymbol{\mu}(\boldsymbol{q})\cdot\Big[\boldsymbol{F}^{\rm pot}(\boldsymbol{q}) + \boldsymbol{F}^{\rm ran}(\boldsymbol{q},t)\Big]\ , \tag{7-2}$$

where the *mobility* tensor $\boldsymbol{\mu}(\boldsymbol{q})$ is the inverse of the dissipation tensor $\boldsymbol{\gamma}(\boldsymbol{q})$. This equation is recognized as that governing *Brownian motion*, albeit in a scenario more complicated than the standard one. Whereas the standard Brownian motion concerns a heavy particle immersed in an isotropic fluid without any external forces acting, the above equation includes the force from the potential $U(\boldsymbol{q})$ and also allows the mobility tensor $\boldsymbol{\mu}(\boldsymbol{q})$ to be anisotropic; both depend on the "position" $\boldsymbol{q}$. Moreover, the dimensionality of the space may differ from three (for the three-quadratic-surface shape family, which contains five shape parameters, the motion takes place in five dimensions).

The Smoluchowski equation in the form (7-2) may be used to propagate the shape for a brief time interval Δt. The accumulated shape change then amounts to

$$\Delta\boldsymbol{q} \;\equiv\; \int_t^{t+\Delta t}\dot{\boldsymbol{q}}(t')\,dt' \;\approx\; \boldsymbol{\mu}(\boldsymbol{q})\cdot\left[\boldsymbol{F}^{\rm pot}(\boldsymbol{q})\,\Delta t + \int_t^{t+\Delta t}\boldsymbol{F}^{\rm ran}(\boldsymbol{q},t')\,dt'\right]\ . \tag{7-3}$$

Because of the force $\boldsymbol{F}^{\rm ran}$ is random, the accumulated shape change $\Delta\boldsymbol{q}$ is a stochastic quantity characterized by a distribution function $P(\Delta\boldsymbol{q})$. The average shape change is due solely to the the potential (because the average of the random force is zero),

$$\prec\Delta\boldsymbol{q}\succ \equiv\ \int\Delta\boldsymbol{q}\,P(\Delta\boldsymbol{q})\,d\boldsymbol{q} \;\approx\; \boldsymbol{\mu}(\boldsymbol{q})\cdot\boldsymbol{F}^{\rm pot}(\boldsymbol{q})\,\Delta t\ . \tag{7-4}$$

The mean "displacement" (*i.e.* the mean shape change), $\Delta\boldsymbol{q}$, is thus generally *not* in the direction of the driving force from the potential, $\boldsymbol{F}^{\rm pot}$, but is modified due to the fact that the friction affects the different shape parameters differently. Furthermore, the diffusion of the shape trajectory, $\boldsymbol{q}(t)$, is due entirely to the random force,

$$\begin{aligned}\prec\Delta q_i\Delta q_j\succ \;&\equiv\; \int\Delta q_i\,\Delta q_j\,P(\Delta\boldsymbol{q})\,d\boldsymbol{q} \qquad (7\text{-}5)\\ &=\; \boldsymbol{\mu}(\boldsymbol{q})\cdot\int_t^{t+\Delta t}\int_t^{t+\Delta t}\langle\boldsymbol{F}^{\rm ran}(\boldsymbol{q},t')\,\boldsymbol{F}^{\rm ran}(\boldsymbol{q},t'')\rangle\,dt'dt''\cdot\boldsymbol{\mu}(\boldsymbol{q}) \;\approx\; 2T\boldsymbol{\mu}(\boldsymbol{q})\,\Delta t\ ,\end{aligned}$$

where we have used Eq. (2-8) for the correlation function of the random force. Thus the accumulated covariance between the changes in two shape parameters is proportional to the corresponding element of the mobility tensor, μ_{ij}, as well as to the prevailing nuclear temperature.

To simulate the Smoluchowski equation (7-2), it is convenient to diagonalize the mobility tensor. Let $\{\boldsymbol{\chi}^{(n)}\}$ be its eigenvectors normalized such that $\boldsymbol{\chi}^{(n)}\cdot\boldsymbol{\chi}^{(n)}$ is the eigenvalue μ_n,

$$\boldsymbol{\mu}(\boldsymbol{q}) = \sum_{n=1}^{N} \boldsymbol{\chi}^{(n)}(\boldsymbol{q})\,\boldsymbol{\chi}^{(n)}(\boldsymbol{q})^{\dagger}: \quad \mu_{ij}(\boldsymbol{q}) = \sum_{n=1}^{N} \chi_i^{(n)}(\boldsymbol{q})\,\chi_j^{(n)}(\boldsymbol{q}) \ . \tag{7-6}$$

The change in the shape parameter $\boldsymbol{q}$ accumulated during a brief time Δt is then given by

$$\Delta\boldsymbol{q} \ = \ \sum_{m=1}^{N} \Delta\boldsymbol{q}^{(m)} \ , \quad \Delta\boldsymbol{q}^{(m)} \ = \ \sum_{n=1}^{N} \boldsymbol{\chi}^{(n)} \left[\Delta t\,\boldsymbol{\chi}^{(n)}\cdot\boldsymbol{F}^{\rm pot} + \sqrt{2T\Delta t}\ \xi_n^{(m)}\right] \ , \tag{7-7}$$

where $\{\xi_n^{(m)}\}$ are random numbers drawn from a distribution with zero mean and unit variance.

It is instructive to investigate how sensitive the extracted fragment mass distribution is to the detailed structure of the dissipation tensor. For example, if $\boldsymbol{\gamma}(\boldsymbol{q})$ is the dissipation tensor obtained with the one-body wall formula (6-3), but renormalized such that its N eigenvalues $\{\gamma_n(\boldsymbol{q})\}$ are unity on average, $\sum_n \gamma_n = N$ (N is five for the 3QS shape family), then a more isotropic dissipation tensor $\tilde{\boldsymbol{\gamma}}(\boldsymbol{q})$ is defined by modifying the eigenvalues as follows,

$$\tilde{\gamma}_n^{(f)}(\boldsymbol{q}) \ \equiv \ [\gamma_n(\boldsymbol{q}) + f]/[1+f] \ , \quad 0 \le f \le \infty \ . \tag{7-8}$$

Figure 7-2 illustrates the dependence of the mass distribution on the anisotropy of $\boldsymbol{\gamma}$:

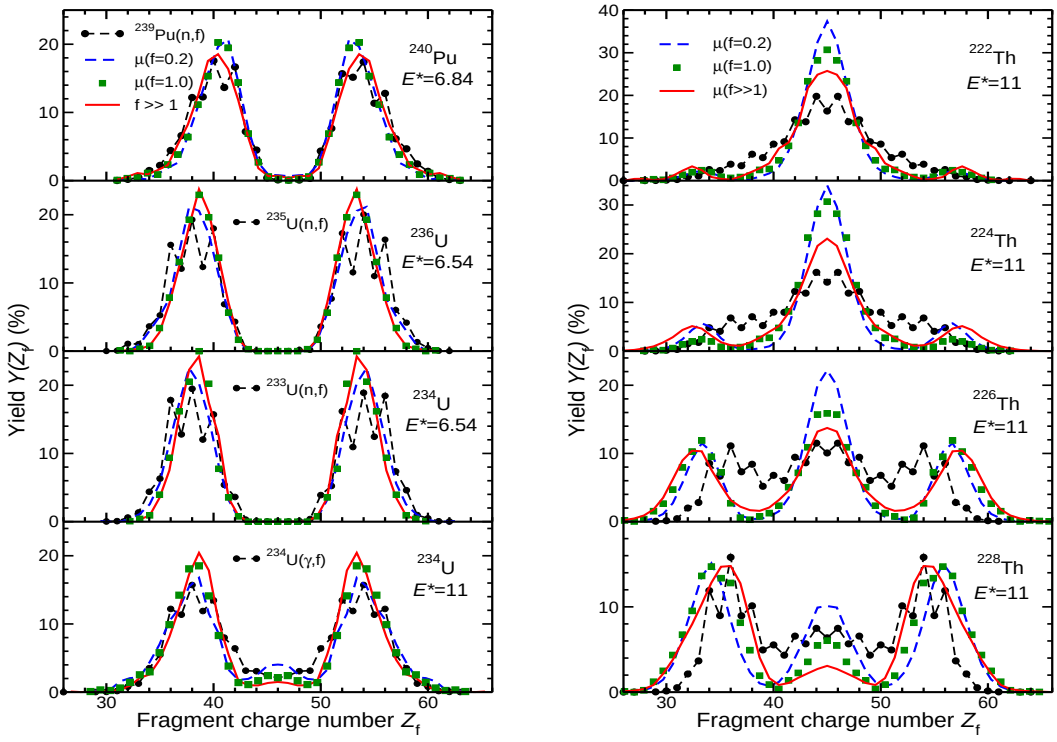

Figure 7-2: Fragment charge distributions obtained by simulating the Smoluchowski equation with (7-7) using dissipation tensors $\boldsymbol{\gamma}(\boldsymbol{q})$ that have different degrees of structure, as governed by the parameter f (see Eq. (7-8)), as well as the corresponding experimental data (solid dots). The value $f = \infty$ yields a totally isotropic dissipation tensor, $\gamma_{ij} \sim \delta_{ij}$, and the corresponding results agree closely with those obtained by means of the Metropolis lattice walk (see Sect. 7.2). (From Ref. [30].)

7.2 Metropolis lattice walk

Although the Smoluchowski evolution is easy to simulate numerically using Eq. (7-7) [30], it does require that *both* the potential $U(\boldsymbol{q})$ *and* the dissipation tensor $\boldsymbol{\gamma}(\boldsymbol{q})$ are known. While $U(\boldsymbol{q})$ appears to be quantitatively quite well understood nowadays, our knowledge of $\boldsymbol{\gamma}(\boldsymbol{q})$ is still only fairly rudimentary. But some observables are not so sensitive to the details of $\boldsymbol{\gamma}(\boldsymbol{q})$ (see Fig. 7-2) so, for explorative purposes, one may make simplifying assumptions about it.

In particular, if $\boldsymbol{\gamma}(\boldsymbol{q})$ is isotropic, $\gamma_{ij}(\boldsymbol{q}) = \gamma(\boldsymbol{q})\,\delta_{ij}$, then the transport process reduces to a standard random walk [30, 31] and the increments of the shape parameters are readily obtained,

$$\Delta q_i \;=\; \mu(\boldsymbol{q})F_i(\boldsymbol{q})\Delta t + \sqrt{2T\mu(\boldsymbol{q})\Delta t}\;\xi_i \;, \quad \mu(\boldsymbol{q}) \equiv 1/\gamma(\boldsymbol{q}) \;, \tag{7-9}$$

where $\{\xi_i\}$ are random numbers drawn from a distribution with zero mean and unit variance. If the potential energy U is known for any value of the shape parameter $\boldsymbol{q}$, then the local force $\boldsymbol{F}$ can be obtained as the corresponding gradient, $F_i(\boldsymbol{q}) = -\partial U(\boldsymbol{q})/\partial q_i$.

However, if the potential energy is available only on a discrete lattice, as that employed for the 5D tabulation [12] (see Fig. 4-12), then one must resort to a suitable interpolation scheme, such as the pentalinear method [30]. Alternatively, one may restrict the possible values of $\boldsymbol{q}$ to those appearing in the lattice. As it turns out [30, 31], such a discrete transport process is equivalent to performing a *Metropolis* walk on the potential-energy lattice. Introduced for 7-a
the purpose of exploring a complicated parameter space according to the appropriate statistical weight [32], $W(\boldsymbol{q}) \sim \exp(-U(\boldsymbol{q})/T)$ for a thermal distribution, the Metropolis walk simulates a simple diffusion process through the lattice. When the system has arrived at a certain lattice site, it selects one of the neighboring sites at random and decides whether to move there next (or stay at the current site) based on the associated change in potential energy: If the potential step is "downhill", *i.e.* $\Delta U < 0$, then the step is taken; but if ΔU is positive then the step is taken only with the corresponding thermal probability, $\exp(-\Delta U/T)$.

The Metropolis lattice walk, combined with a bias potential of the form $U_{\rm bias}(\boldsymbol{q}) = Q_0^2/Q^2$, provies a simple and powerful means for obtaining approximate fission-fragment mass distributions in an essentially parameter-free manner. Figure 7-3 shows the very first results [31] obtained by this method which has since then been extensively benchmarked [33].

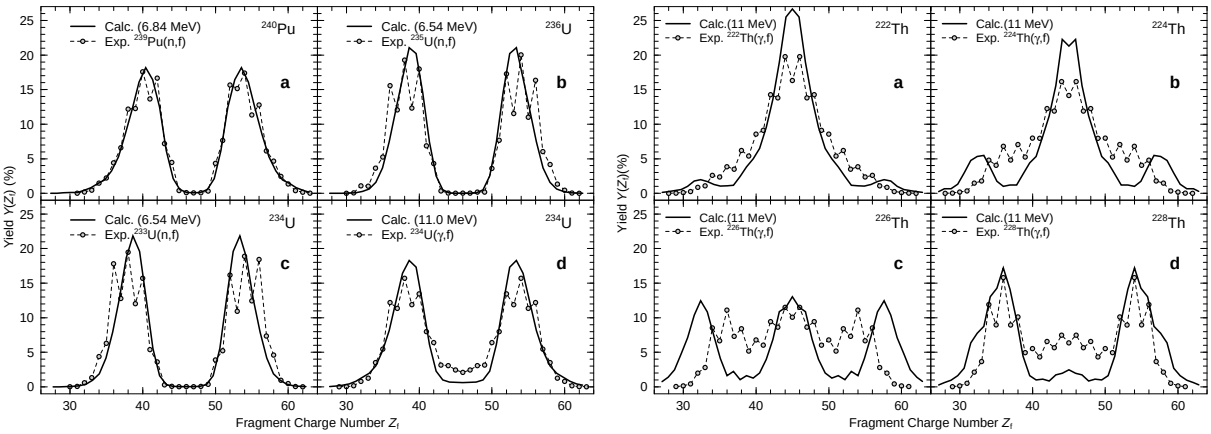

Figure 7-3: The first fission-fragment charge distributions obtained by means of the Metropolis lattice walk [31] (solid), together with the corresponding experimental data (dashed). [From Ref. [31].]

7.3 Langevin simulations

Nuclear fission dynamics is sensitive to a variety of physical quantities, particularly the potential energy of deformation, the associated inertial mass, and the dissipation mechanism. Valuable insight into these important aspects of the nuclear many-body system may therefore be obtained once a reliable dynamical treatment has been developed. Offering a physically well-based formal framework for such studies, Langevin simulations of nuclear shape dynamics have been employed extensively and have generally speaking met with a large degree of success (for a few examples, see Refs. [34, 35, 36, 37]).

However, those studies have largely been restricted to higher energies where microscopic effects are unimportant. The macroscopic limit has the dual advantage of the relative ease with which the potential can be calculated and the fact that fewer shape degrees of freedom are needed, thus reducing the dimensionality of the parameter space.

Low-energy nuclear shape dynamics poses a significantly larger challenge, because it is essential to include the microscopic corrections, at least for the potential energy, and a minimum of five different types of deformation must be considered for fission. But significant progress has been made recently and it is now possible to simulate the Langevin equation (Sect. 2) within the three-quadratic-surface shape family (Sect. 3) using the macroscopic-microscopic potentials (Sect. 4), the incompressible irrotational inertial masses obtained in the Werner-Wheeler approximation (Sect. 5), and a scaled one-body wall-plus-window dissipation (Sect. 6).

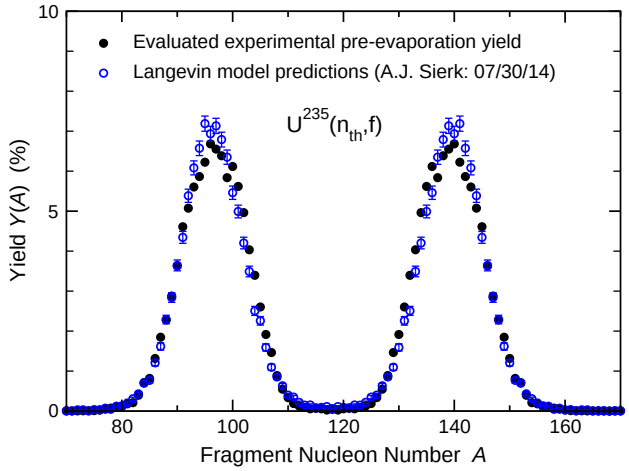

Figure 7-4: The fragment mass distribution for ^{235}U(n_{th},f) as resulting from preliminary Langevin calculations (open circles) together with the experimentally deduced distribution (solid dots). The initial nuclear shape parameters and the associated (outwards directed) momenta were sampled from a distribution located just beyond the third saddle and they were then propagated until shortly before scission. (This figure was kindly provided by Arnie Sierk [38].)

The computational effort required for a full Langevin simulation of fission is about two orders of magnitude larger than that needed for solving the Smoluchowski equation. But it should be recognized that whereas the Smoluchowski treatment yields only the shape evolution (*i.e.* the *path* through the shape space, without a clock and hence no velocities), the Langevin treatment provides the full dynamical information $(\boldsymbol{q}(t), \dot{\boldsymbol{q}}(t))$ and thus makes it possible to also extract fragment kinetic energies, in addition to fragment masses - a very important capability. Thus is has now become possible to carry out numerical simulations of low-energy fission dynamics and obtain useful event samples in a reasonable time.

Acknowlegdements: I am grateful to Peter Möller and Arnie Sierk for their careful reading of these notes and their many helpful comments.

References

[1] O. Hahn and F. Straßmann, Naturwissenschaften 27 (1939) 11.

[2] L. Meitner and O.R. Fritsch, Nature 143 (1939) 239.

[3] N. Bohr and J.A. Wheeler, Phys. Rev. 56 (1939) 426.

[4] N. Bohr, Nature 137 (1936) 344.

[5] N. Bohr, Lecture to the Chemical and Physical Society of University College, London, February 11, 1936 [reported in *News and Views*, Nature 137 (1936) 351].

[6] J.R. Nix, Nucl. Phys. A 130 (1969) 241.

[7] J.R. Nix, Ann. Rev. Nuc. Sci. 22 (1972) 65.

[8] W.D. Myers and W.J. Swiatecki, Nucl. Phys. 81 (1966) 1.

[9] C.F. von Weizsäcker, Zeit. Phys. 96 (1935) 431.

[10] H.A. Bethe and R.F. Bacher, Rev. Mod. Phys. 8 (1936) 82.

[11] P. Möller, J.R. Nix, W.D. Myers, and W.J. Swiatecki, Atomic Data and Nuclear Data Tables 59 (1995) 185.

[12] P. Möller, A.J. Sierk, T. Ichikawa, A. Iwamoto, R. Bengtsson, H. Uhrenholt, and S. Åberg, Phys. Rev. C 79 (2009) 064304.

[13] H.J. Krappe and J.R. Nix, Proc. Third IAEA Symp. on Physics and Chemistry of Fission, Rochester, 1973 (IAEA, Vienna, 1974) paper IAEA-SM-174/12, vol. 1, p. 159.

[14] J. Blocki, J. Randrup, W.J. Swiatecki, and C.F. Tsang, Ann. Phys. 105 (1977) 427.

[15] H.J. Krappe, J.R. Nix, and A.J. Sierk, Phys. Rev. Lett. 42 (1978) 215; Phys. Rev. C 20 (1978) 992.

[16] K.T.R. Davies and J.R. Nix, Phys. Rev. 14 (1976) 1977.

[17] M. Bolsterli, E.O. Fiset, J.R. Nix, J.L. Norton, Phys. Rev. C 5 (1972) 1050.

[18] H. Schatz, S. Gupta, P. Möller, M. Beard, E.F. Brown, A.T. Deibel, L.R. Gasques, W.R. Hix, L. Keek, R. Lau, A.W. Steiner, M. Wiescher, Nature 505 (2014) 62.

[19] V.M. Strutinsky, Nucl. Phys. 95 (1967) 420; 122 (1968) 1.

[20] M. Brack, J. Damgaard, A.S. Jensen, H.C. Pauli, V.M. Strutinsky, and C.Y. Wong, Rev. Mod. Phys. 44 (1972) 320.

[21] P. Möller and J.R. Nix, Nucl. Phys. A 536 (1992) 20.

[22] H. Olofsson, R. Bengtsson, and P. Möller, Nucl. Phys. A 784 (2007) 104.

[23] P. Möller, Nucl. Phys. A 192 (1972) 529.

[24] P. Möller, D.G. Madland, A.J. Sierk, and A. Iwamoto, Nature 409 (2001) 785.

[25] T. Ichikawa, A. Iwamoto, P. Möller, and A.J. Sierk, Phys. Rev. C 86 (2012) 024610.

[26] J.R. Nix, UCRL-17958 (1968).

[27] K.T.R. Davies, A.J. Sierk, and J.R. Nix, Phys. Rev. 13 (1976) 2385.

[28] J. Blocki, Y. Boneh, J.R. Nix, J. Randrup, M. Robel, A.J. Sierk, and W.J. Swiatecki, Ann. Phys. 113 (1978) 330.

[29] A.J. Sierk and J.R. Nix, Phys. Rev. C 21 (1980) 982.

[30] J. Randrup, P. Möller, and A.J. Sierk, Phys. Rev. C 84 (2011) 034613.

[31] J. Randrup and P. Möller, Phys. Rev. Lett. 106 (2011) 132503.

[32] N. Metropolis, A.W. Rosenbluth, M.N. Rosenbluth, A.H. Teller, and E. Teller, J. Chem. Phys. 26 (1953) 1087.

[33] J. Randrup and P. Möller, Phys. Rev. C 88 (2011) 034613.

[34] G. Chaudhuri and S. Pal, Phys. Rev. C 63 (2001) 064603.

[35] A.V. Karpov, P.N. Nadtochy, D.V. Vanin, and G.D. Adeev, Phys. Rev. C 63 (2001) 054610.

[36] P.N. Nadtochy, A. Kelić and K.-H. Schmidt, Phys. Rev. C 75 (2007) 064614.

[37] K. Mazurek, C. Schmitt, P.N. Nadtochy, M. Kmiecik, A. Maj, P. Wasiak, and J.P. Wieleczko, Phys. Rev. C 88 (2013) 054614.

[38] A.J. Sierk, Private communication (August 2014).

Exercises:

2-a: We recall that $p_i = \sum_j M_{ij}\dot{q}_j$ and first note that $\sum_j B_{ij}M_{jk} = \delta_{ik}$ implies that

$$0 = \frac{\partial}{\partial q_\ell}\sum_j B_{ij}M_{jk} = \sum_j \frac{\partial B_{ij}}{\partial q_\ell}M_{jk} + \sum_j B_{ij}\frac{\partial M_{jk}}{\partial q_\ell} \ .$$

It then readily follows that

$$\begin{aligned}\sum_{jk} p_j \frac{\partial B_{jk}}{\partial q_i}p_k &= \sum_{\ell jkm} \dot{q}_\ell M_{\ell j}\frac{\partial B_{jk}}{\partial q_i}M_{km}\dot{q}_m = -\sum_{\ell jkm}\dot{q}_\ell M_{\ell j}B_{jk}\frac{\partial M_{km}}{\partial q_i}\dot{q}_m \\ &= -\sum_{\ell km}\dot{q}_\ell\,\delta_{\ell k}\frac{\partial M_{km}}{\partial q_i}\dot{q}_m = -\sum_{\ell m}\dot{q}_\ell\frac{\partial M_{\ell m}}{\partial q_i}\dot{q}_m = -\sum_{jk}\dot{q}_j\frac{\partial M_{jk}}{\partial q_i}\dot{q}_k \ .\end{aligned}$$

2-b: Transport in the harmonic approximation: Verify Eq. (2-15). Insert the gaussian ansatz $P(x,t) \sim \exp(-(x-\bar{x})^2/2\sigma^2)/\sigma$ into the Fokker-Planck equation (2-12) and evaluate the left-hand side minus the right-hand side, using $\partial_t\bar{x} = V(\bar{x}) = -\bar{x}/t_0$ and $\partial_t\sigma^2 = 2D - 2\sigma^2/t_0$,

$$\begin{aligned}&\left\{\partial_t P(x,t) + \partial_x[V(x)P(x,t)] - \partial_x^2[D(x)P(x,t)]\right\}/P(x,t) \\ =\ &\left(\frac{x-\bar{x}}{\sigma^2}\,\partial_t\bar{x} + \frac{(x-\bar{x})^2}{2\sigma^4}\,\partial_t\sigma^2 - \frac{\partial_t\sigma^2}{2\sigma^2}\right) + \left(\frac{x}{t_0}\frac{x-\bar{x}}{\sigma^2} - \frac{1}{t_0}\right) + \left(\frac{D}{\sigma^2} - D\frac{(x-\bar{x})^2}{\sigma^4}\right) \\ =\ &-\frac{x-\bar{x}}{\sigma^2}\frac{\bar{x}}{t_0} + \frac{(x-\bar{x})^2}{2\sigma^4}(2D - \frac{2\sigma^2}{t_0}) - \frac{D}{\sigma^2} + \frac{1}{t_0} + \frac{x}{t_0}\frac{x-\bar{x}}{\sigma^2} - \frac{1}{t_0} + \frac{D}{\sigma^2} - D\frac{(x-\bar{x})^2}{\sigma^4} \ = \ 0 \ .\end{aligned}$$

4-a: Formally, the shell-correction method is based on the so-called *Strutinsky energy theorem* which states that the variation of the total many-body energy with respect to the occupation n_i of a given quasi-particle state i is equal to the associated quasi-particle energy, $\delta E/\delta n_i = \epsilon_i$, *i.e.* $\delta E = \sum_i \epsilon_i \delta n_i$. This feature can be illustrated by a classical gas of particles with pairwise interactions, each particle having the weight n_i,

$$E = \sum_i \frac{p_i}{2m_i}n_i + \tfrac{1}{2}\sum_{ij} W(r_{ij})n_i n_j \ \ \Rightarrow \ \ \frac{\delta E}{\delta n_i} = \frac{p_i^2}{2m_i} + \sum_j W(r_{ij})n_j = \epsilon_i \ .$$

The actual (bunched) density of states, $g_0(\epsilon) = \sum_i \mathrm{g}_i\delta(\epsilon - \epsilon_i)$ can be thought of as resulting from a variation of the smooth state density $\tilde{g}(\epsilon)$, $g_0(\epsilon) = \tilde{g}(\epsilon) + \delta g(\epsilon)$. Furthermore, changing the occupancy of states with energy ϵ is equivalent to changing the density of states at that energy, so the change in the many-body energy E_A is then given by Eq. (4-17),

$$\delta E_A = \int^\lambda \epsilon\,\delta g(\epsilon)\,d\epsilon = \int_{-\infty}^\lambda \epsilon\,[g_0(\epsilon) - \tilde{g}(\epsilon)]\,d\epsilon = \sum_i \epsilon_i \mathrm{g}_i - \int_{-\infty}^\lambda \epsilon\tilde{g}(\epsilon)d\epsilon \ .$$

4-b: If two well-separated nuclei, A and B, are in mutual chemical equilibrium, *i.e.* their Fermi levels are equal, $\tilde\lambda_A = \tilde\lambda_B$, then the total shell energy for the combined dinuclear system, C, is the sum of the shell energies for each of the two individual systems.

Note first that the eigenstates $\{\psi_\nu\}$ for the combined potential, $V_C\boldsymbol{r}) = V_A(\boldsymbol{r}) + V_B(\boldsymbol{r})$, consist of those for the potential $V_A(\boldsymbol{r})$, $\{\psi_i\}$, together with those for the potential $V_B(\boldsymbol{r})$, $\{\psi_j\}$. The total density of states is therefore the sum of the two separate state densities,

$$g_C(\epsilon) = \sum_\nu \mathrm{g}_\nu \delta(\epsilon-\epsilon_\nu) = \sum_i \mathrm{g}_i^A \delta(\epsilon-\epsilon_i) + \sum_j \mathrm{g}_j^B \delta(\epsilon-\epsilon_j) = g_A(\epsilon) + g_B(\epsilon)\ .$$

The same is then true for the smooth state density,

$$\tilde g_C(\epsilon) = [\xi * g_C](\epsilon) = [\xi * (g_A+g_B)](\epsilon) = [\xi * g_A](\epsilon) + [\xi * g_B](\epsilon) = \tilde g_A(\epsilon) + \tilde g_B(\epsilon)\ ,$$

where $*$ denotes convolution. Consequently the shell energies are additive,

$$\begin{aligned}
\delta E^{(C)}_{\rm shell} &= E^C - \tilde E^{(C)} = \sum_\nu \mathrm{g}_\nu\epsilon_\nu - \int_{-\infty}^{\tilde\lambda_C} \epsilon\,\tilde g_C(\epsilon)\,d\epsilon \\
&= \sum_i \mathrm{g}_i^A\epsilon_i - \int_{-\infty}^{\tilde\lambda_A} \epsilon\,\tilde g_A(\epsilon)\,d\epsilon \ +\ \sum_j \mathrm{g}_j^B\epsilon_j - \int_{-\infty}^{\tilde\lambda_B} \epsilon\,\tilde g_B(\epsilon)\,d\epsilon \\
&= \left(E^{(A)} - \tilde E^{(A)}\right) + \left(E^{(B)} - \tilde E^{(B)}\right) \ =\ \delta E^{(A)}_{\rm shell} + \delta E^{(B)}_{\rm shell}\ .
\end{aligned}$$

7-a: The shape evolution generated by the Smoluchowski equation can be simulated exactly by a Metropolis walk when the dissipation tensor $\boldsymbol{\gamma}$ is aligned with the lattice, $\gamma_{ij}(\boldsymbol{q}) = \gamma_i(\boldsymbol{q})\delta_{ij}$. First note that when $\boldsymbol{\gamma}$ is aligned then each lattice direction may be considered separately.

In the discrete treatment, the step size is fixed by the lattice spacing Δ, and we need to know the probabilities for taking a forward or backward step during a brief time interval Δt, $P_\pm = \nu_\pm\Delta t$. The associated Fokker-Planck transport coefficients V and D, which express the rate at which the mean location changes and half the rate at which the variance in the location grows, in the considered lattice direction, are therefore given by

$$V = (\nu_+ - \nu_-)\Delta = \mu F\ ,\ \ D = \tfrac12(\nu_+ + \nu_-)\Delta^2 = \mu T\ .$$

Here F is the force in the considered direction and $\mu = 1/\gamma$ is the mobility in that direction; these are both insensitive to Δ. The above relations can readily be solved for the rates,

$$\nu_\pm \ =\ \frac{\mu}{\Delta^2}\left[T \pm \tfrac12 F\Delta\right] \ \approx\ \frac{\mu}{\Delta^2}\left[T \mp \tfrac12\Delta U\right]\ ,$$

where $\Delta U \approx -F\Delta$ is the change in the potential when the position is increased by Δ. So

$$\frac{P_+}{P_-} \ =\ \frac{\nu_+}{\nu_-} \ =\ \frac{T - \frac12\Delta U}{T + \frac12\Delta U} \ \approx\ \mathrm{e}^{-\Delta U/T}\ .$$

This is precisely what characterizes the Metropolis procedure: If the proposed step lowers the potential then it is accepted unconditionally and otherwise it is accepted with the probability $\exp(-\Delta U/T)$. In either case, the ratio between the forward and backward step probabilities equals $\exp(-\Delta U/T)$.

Corrections, additions, modifications (relative to the version dated September 3, 2014):

1. Eq. (2-1) should be

$$\mathcal{L}(\boldsymbol{q},\dot{\boldsymbol{q}}) \;=\; \tfrac{1}{2}\dot{\boldsymbol{q}}\cdot\boldsymbol{M}\cdot\dot{\boldsymbol{q}} - U(\boldsymbol{q}) \;=\; \tfrac{1}{2}\sum_{i,j}^{N}\dot{q}_i\,M_{ij}(\boldsymbol{q})\,\dot{q}_j - U(\boldsymbol{q})\ .$$

2. Eq. (2-6) should be

$$\boldsymbol{F}^{\rm fric}(\boldsymbol{q},\dot{\boldsymbol{q}}) \equiv \langle \boldsymbol{F}^{\rm diss}(\boldsymbol{q},\dot{\boldsymbol{q}})\rangle = -\boldsymbol{\gamma}(\boldsymbol{q})\cdot\dot{\boldsymbol{q}}: \quad F_i^{\rm fric}(\boldsymbol{q},\dot{\boldsymbol{q}}) = \langle F_i^{\rm diss}(\boldsymbol{q},\dot{\boldsymbol{q}})\rangle = -\sum_j \gamma_{ij}(\boldsymbol{q})\,\dot{q}_j\ .$$